Electromagnetic Principles for In Situ Ice Thickness Determination

Field Experiments and Development of New

Methods for Interpretation

Johannes P Lorentzen

Preface

This thesis contains the sum of a year worth of work, stretching over the two last years. It has been a demanding challenge and had a huge learning curve. I do not regret starting this thesis, even though it sometimes has been hard not setting the whole thing on fire. The thesis started as a simple question,

> *"Can you find the internal properties of an ice ridge using electromagnetic methods?"*

and quickly grew from there. As the work progressed more and more questions arose, and the complexity of the original question became clear. The question was not trivia, and many solutions where proposed. In the end, many ideas did work, and some did not, particularly the attempt with an echo sounder did not fulfill the expectations.

One of the challenges has been the lack of previous work on the topic, only a few articles had touched the subject and none had tried to develop a method. Some inspiration came from the fields of geology and geophysics, where they look at similar problems, but on a completely different scale. It did however allow me to define my own investigation and taught me much about what to do, and not to do, when investigating in the Arctic.

Trondheim, May 15, 2015

Johannes Pippidis Lorentzen

I

Acknowledgements

Summary

During the spring of 2014 fieldwork in three different locations on Svalbard was conducted in order to investigate the application of electromagnetic methods on sea ice and ice ridges. Two validation grids, one transect across Sveasundet, a walkabout, an ice ridge and 8 ice cores have been measured. Results show an average thickness less than one meter for all but the ice ridge, which was 1,9 meters at the thickest point.

Simulation based calculation of the relationship between the measured apparent conductivity and the level ice thickness, using MarcoAir, show great accuracy and potential. The sea ice conductivity profile is shown to have great effect on the calculated thickness, and this becomes more and more apparent as the thickness of the ice increases. This effect is shown, by using a simple quasi-2D model of an ice ridge, to hold for ice ridges. Investigation into the potential methods of estimating internal structures of ice ridges show that there are great potential in using simulation and modelling in combination with inversion, in order to assess these properties.

Sammendrag

I løpet av våren 2014 ble feltarbeid gjennomført på tre forskjellige lokasjoner på Svalbard. Hensikten var å undersøke bruk av elektromagnetiske metoder på sjøis og skrugarder. Det ble foretatt 2 valideringsnett, en tilfeldig vandring, en linje over Sveasundet samt målinger av en skrugard med EM31 instrumentet. En gjennomsnittlig istykkelse ble funnet til under en meter, og den maksimale tykkelsen på skrugarden var 1,9 meter. Det ble også målt 8 iskjerner fra de forskjellige områdene.

Utregninger basert på simulering og teori viser at forholdet mellom målt "oppfattet konduktivitet" og tykkelsen på flat is, kan gjenskapes ved hjelp av MarcoAir og iskjernemålinger. Konduktivitetsprofilen til flat is er vist å ha stor påvirkning på den kalkulerte tykkelsen, noe som forsterkes når isen blir tykkere. Den samme effekten er påvist for skrugarder ved hjelp av simulering.

Undersøkelse av mulige fremtidige elektromagnetiske metoder viser at det er stort potensiale for å regne ut de interne egenskapene til en skrugard ved bruk av en modell basert simulering.

Table of Contents

List of Tables

List of Figures

Abbreviations

AGF	=	Arctic Geophysics department at UNIS
AT	=	Arctic Technology department at UNIS
CTD	=	"Conductivity, Temperature, Depth", an oceanographic instrument
CRIOS	=	Calving Rates and Impact on Sea Level. A research project
EM31	=	EM31-Mk2-Ice
GPS	=	Global Positioning System
HCP	=	Horizontal coplanar
NTNU	=	Norwegian University of Science and Technology
ppt	=	Parts per thousand
psu	=	Practical salinity units
RMS	=	Root mean square
RV	=	Research vessel
SAR	=	Synthetic aperture radar
UNIS	=	The University Centre in Svalbard
VCP	=	Vertical coplanar

Chapter 1

Introduction

The Arctic region has been a location for study and exploration for a long time, captivating and distinctive. Most of the Arctic is covered by sea ice, $1,6 \cdot 10^6 \text{km}^2$ in 2012, but the area covered is decreasing, and the melting season is generally longer (Stroeve et al., 2014). One of the more characteristic parts of the sea ice cover is the ice ridges, large piles and walls of ice in an otherwise flat environment. An ice ridge is defined as:

> **[Ice] Ridge:** A line or wall of broken ice forced up by pressure. May be fresh or weathered. The submerged volume of broken ice under a ridge, forced downwards by pressure, is termed an ice keel. (WMO, 2009)

by the World Meteorological Organization, and shown in Figure 2.3. As the extent of the Arctic sea ice is lessening steadily each year, the activity in Arctic waters are increasing (Berkman and Young, 2009). The shipping industry are looking at an Arctic passage to Asia, the oil and gas industry looks at the possibility of extracting the oil and gas trapped beneath the Arctic ocean (Palmer and Croasdale, 2012), the cruise industry are ever pushing the boundaries to deliver exiting vacations (Hall, 2001). the fishing industry are looking for new fishing possibilities and the mining industry are interested in the mineral reserves. All of these frontier industries need to understand the ice processes and characteristics in to operate safely in the Arctic.

The oil and gas industry need to know the stress on their platforms and offshore structures to operate. The design of these structures need to be scaled in order to withstand not only the hearse weather and the level ice drift, but also the ice ridges. Ice ridges can be multiple times larger than the level ice field where they are formed, and can such potentially exert much more force on the structures. However, as ice ridges are not solid blocks of ice, their internal structure have a large impact on the force on the structures (Løset et al., 2006). If there is knowledge about the ice that is about to hit the structure, one can decide whether or not one need to disengage the operation or not. A wrong decision can cost the company substantial amounts. Worse, if one should have disengaged, the cost can

be counted in the billions, and could have catastrophic impacts on the environment. The shipping, fishing, and cruise industry need to know the strength and distribution of ridges for navigation and operation.

The importance of ice ridges on the drift of sea ice is also great, as the sail of the ridge works as a sail in the wind; and the keel is reaching further down into the sea and thereby affected by forces in other directions due to the Ekman layer (Arya, 1973). This along many other aspects, makes the understanding of ice ridges as a critical part of the understanding of operation in the Arctic.

The impact of Arctic sea ice on the climate is shown to be great (Thomas and Dieckmann, 2010), and have wide spread effects. Climate studies show that ice ridges increases the turbulence of the lower layer atmosphere (Garbrecht et al., 1999), incensing heat transfer, among other effects.

One of the aspects of ice ridges, which is most difficult to measure, is the internal structure. As these ridges are semi-chaotic piles of ice, the structure is difficult to model and hard to measure. A way of quantify some of these internal properties from an electromagnetic; non-intrusive methods would benefit the climate research and industry alike.

1.1 Questions and scope

While the idea of using electromagnetic methods to quantify the internal properties of ice ridges is easy to propose, the application is not. The two main reasons for this is a) the problem not to have a non-unique solution and demand a huge amount of computational time to solve, known as the inversion problem, b) the normal approximations for electromagnetic geophysical explorations is invalid due to the high conductivities of the ocean and brine, and the physical scale of the ridges. In order to approach this problem, I have divided it into the following questions:

Q1: *How does the level ice conductivity profile affect the response of electromagnetic measurements[1], and how does this affect the readings from an ice ridge?*

Q2: *Is it possible to make a 3D inversion model to estimate the internal structure of an ice ridge?*

Q3: *How can conductivity models of ice ridges improve the estimation of ridge thickness and internal structures?*

Q4: *Can an automatic system analyse measurements, identify ridges and calculate the internal properties?*

In order to shed some light on these questions, a combination of field research, simulations and calculations, and literature review has been applied. The fieldwork has been made

---

[1]Using the EM31 instrument, see Section 2.3.

during a stay at the University Centre on Svalbard (UNIS). Svalbard is located north of Norway, and the main city, Longyearbyen is at 78.14° North, as shown in Figure 1.1. The red area is Svalbard, where the main island is called Spitsbergen.
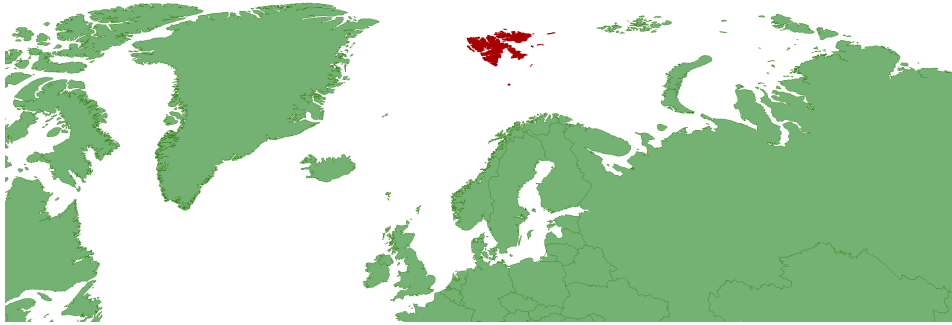
Figure 1.1: Map showing Svalbard (red) location north of Norway.

1.2   Previous Research

Not much research has been done on the electromagnetically response of ice ridges. However, a substantial amount has been done on ice ridges in general. Large studies on the shape and size of the ridges (Strub-Klein and Sudom, 2012; Timco and Burden, 1997). These studies gives the required background to make a model of ice ridges, and recognize ridges on a large data set. Bjerkås (2006) mounted an electromagnetic device, a laser device and a sonar on a lighthouse in addition to pressure sensors on the structure. Much has also been done regarding internal processes and consolidation of the ridges (Høyland, 2002a,b), and Parmeter and Coon (1972) propose a model of ice ridge formation in sea ice. A full life story of a first year ice ridge have been compiled by Leppäranta et al. (1995), where they have described all the stages of a first year ice ridge.

When it comes to level ice, and ice in general, much more research have been conducted and multiple books on the subject have been published. The research into the brine, temperature and mechanical properties of sea ice are relatively well known, and treated in detail in Thomas and Dieckmann (2010). The electromagnetically properties of level ice has however been less examined. Much of the research in this field is from the viewpoint of remote sensing (Stogryn and Desargant, 1985), at frequencies much higher than the ones used in geophysical exploration, and can therefore not be applied. For lower frequencies (0-10kHz) there are some investigations that have been made, most noticeably Haas et al. (1997) set the standard. Thyssen et al. (1974); Morey et al. (1984); Reid et al. (2006b) and Ingham et al. (2012) has also made investigation into the topic.

Many of the articles regarding level ice also raises the questions of ice ridges, and how to measure them. Reid et al. (2003) made a short analysis on the electromagnetic response of ice ridges, modelling the response with a software called MarcoAir. They found that the electromagnetic method gives a highly smoothed picture of the ice ridge, and that the

elevation of the instrument has an influence on this. The same group (Reid et al., 2006a), did more analysis on the problem, with focus on airborne systems. Similar work have also been done by Worby et al. (1999).

Tateyama et al. (2004) made a conductivity model of the ice and looked into the application of the salinity and temperature as a way of calculating the ice total thickness. Uto et al. (2006) further developed the method, outlining a model for an semi-empirical calculation of ice thickness. Tateyama et al. (2006) proposes a standard model of the sea ice, using the simulation software PCLOOP. As main users of the electromagnetic measuring devises are the mining industry and geological exploration, a great deal of research have been conducted on similar problems. The main difference from sea ice is the conductivities of the rock and earth is of an order of magnitude less than what is found in sea ice and seawater. It is from this research most of the simulation tools and formulas have their origin. Summaries of the theory and applications from this angle can be found in Nabighian (1987); Telford et al. (1990) and Reynolds (2011).

Chapter 2

Theory

2.1 Sea Ice

The term "sea ice" can be used about all ice that is on the sea, from icebergs to level ice. In this thesis only level ice and level ice compressed into ice ridges will be considered, and referred to as sea ice. "Level ice" can be divided into land fast ice and pack / drift ice and is defined by the World Meteorological Organisation as:

> **Level ice:** Sea ice which has not been affected by deformation. (WMO, 2009)

Land fast ice is sea ice that is frozen or connected to the shore. "Drift ice" is ice that is freely drifting, and can further be divided into three parts, shear zone, marginal zone and central pack. Figure 2.1a show the structure of sea ice.

2.1.1 Formation

The formation of sea ice starts when the sea-air interface cools down to the freezing point. Dependent on the salinity of the sea, this temperature is typically around -1,8°C. The ice formation differs depending on whether the ocean is calm or rough, giving two different structures.

If the ocean is calm, the ice first forms grease ice, a mushy slush. Then these crystals freeze together to form thin sheets called nilas. When these sheets are moved around, due to currents and wind, they are stacked on top of each other. This is called rafting. After some time the ice grows and becomes a more stable sheet, called congelation ice, and have a smooth surface underneath. If the ocean is rough, the crystals form shapes called pancakes. These pancakes are then rafted together and then frozen by a consolidation process. The bottom surface of this type of ice is, unlike the ice formed in calm water, rough.

The rate at which sea ice is growing can be estimated by Stefan's law shown in equation 2.1 (Høyland, 2009), derived by looking at the thermodynamical processes,

$$h_i^2 = h_{i,0}^2 + \frac{2\kappa}{\rho \cdot l} \sum_n (T_f - T_{is}) \tag{2.1}$$

where h_i is current thickness, $h_{i,0}$ is the initial thickness, κ is the thermal conductivity and l is the latent heat. T_f and T_{is} is the freezing point and the average daily ice surface temperature respectively. n is the number of days. This equation can be approximated as the square root of the time passed:

$$h_i \approx \sqrt{t} \tag{2.2}$$
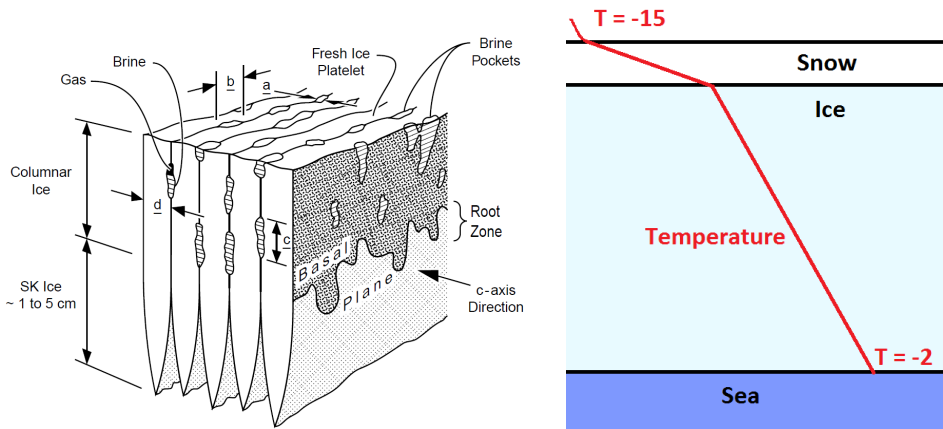
(a) Sea ice structure. The dark and light parts are frozen and seawater interfaces respectively (Kovacs et al., 1996)

(b) Sample temperature profile for level ice with snow on top. The air temperature is -15°C and bottom temperature is -2°C.

Figure 2.1

2.1.2 Temperature

The vertical temperature profile of sea ice is due to the thermodynamical properties of the ice. The profile is dominated by the two environmental factors, sea water temperature, typically -1,8°C, and the air temperature changes with the season and weather. Figure 2.1b shows a simple temperature profile with a snow layer and -1,8°C sea temperature and -15°C air temperature. The extra energy will cause freezing or melting. The illustration is not to scale.

2.1.3 Salinity and Brine

As salt is not a part of the crystal structure of ice, most of the salt in sea ice is found in so-called brine pockets. Brine is a water–salt solution with a high salinity keeping the brine from freezing. These brine pockets are in a temperature equilibrium with the surrounding ice, and move during the lifetime of the ice. The bulk salinity of the ice calculated as the fraction of salt to water in the ice. The vertical profile of the bulk salinity often forms an "C" - shape as described in Eicken (1992) and Thomas and Dieckmann (2010) as shown in Figure 2.2b. Figure 2.2a shows an X-ray micro tomography image of the brine channels and pockets at different temperatures and porosities (Golden et al., 2007). The normal range of salinity is between 1 and 12 ppt for Arctic sea ice, while the sea water is usually between 30 and 34 ppt.

$T = -6°C, \phi = 0.075$ $T = -3°C, \phi = 0.143$

(a) X-ray micro-tomography of brine pockets at different poros-ity (ϕ) and temperature (Golden et al., 2007).

(b) Sample salinity profile from the Weddell sea (Eicken, 1992).
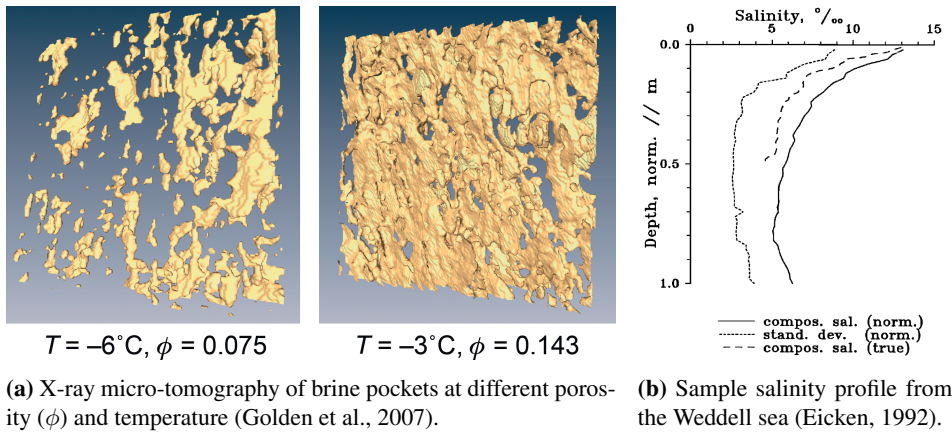
Figure 2.2

2.1.4 Electromagnetical Properties of sea ice

To find the conductivity of the ice, a method outlined in Tateyama et al. (2004) is normally used. The sea ice can be approximated as a sandstone saturated with brine, and then the use of Archie's Law (Archie, 1942) can be applied. The experimental law states that the conductivity of the media can be approximated as the amount of brine present in the host media. Flowingly the sea ice conductivity (σ_I) is given by Equation 2.3.

$$\sigma_I = \sigma_b V_b^m \tag{2.3}$$

where σ_b is the brine conductivity, V_b is the brine volume and m is an empirical constant. Then to derive the conductivity of the ice, these three factors has to be determined. The brine conductivity can be calculated from the temperature as described in Tateyama et al. (2004) by Equation 2.4 that is derived from the work of Stogryn and Desargant (1985).

$$\sigma_b = T_b \exp\left(0.5193 + 0.08755 T_b\right) \qquad (-22.9°C \leq T_b \leq -0.5°C) \tag{2.4}$$

where T_b is the temperature of the brine in °C. The brine volume can be calculated by Equation 2.5 also from Tateyama et al. (2004), originally derived from Frankenstein and Garner (1967).

$$V_b = S_I \cdot (\frac{49.185}{|T_I|} + 0.532) \qquad (-22.9°C \leq T_I \leq -0.5°C) \qquad (2.5)$$

where S_I is the salinity of the ice. The empirical constant m, that Haas et al. (1997) called the 'cementation factor' is found experimentally, and they used 1,75 for their calculation. Others have found it to be between 1,55 for the top and 1,75 close to the ice/water interface (Morey et al., 1984), and 2,2 was found by Thyssen et al. (1974).

2.2 Ice Ridges

An ice ridge or pressure ridge is formed when an ice field is put under pressure, either from compression or shear forces. The pressure forces the ice to break and crumble, lying on top of each other. The process is described in Hopkins and Tuhkuri (1999), and a model is proposed by Parmeter and Coon (1972) where they describe the formation of the ridges. After the initial formation, the seawater between blocks of ice starts to freeze together in the areas close to the waterline. This process is called the consolidation process, it changes the ridge from a loose collection of ice blocks to a more solid structure as described by Høyland (2002a) and Høyland (2002b). The lifecycle of a ridge is described by Leppäranta et al. (1995). If the ridge survives the first year, including the melting season during summer, it is called a multi-year ridge. In this thesis mainly first year ice ridges will be considered. A sketch of a typical first year ridge is shown in Figure 2.3.
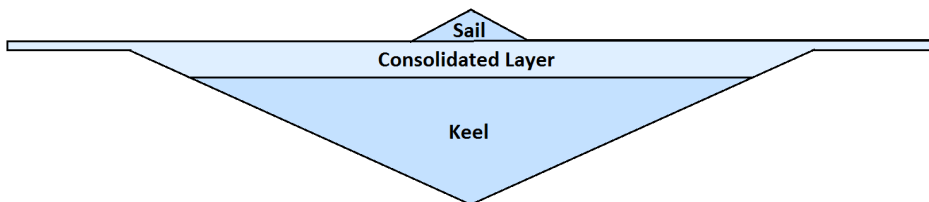
Figure 2.3: Simple sketch of a first year ice ridge.

2.2.1 Structure of ice ridges

An ice ridge is composed of three parts; the rubble on top is called the sail. The sail is in first year ridges is usually loose blocks of ice with air and snow in-between. The height of the sail (h_s) is on average 2 meters, the average elevation ($\bar{h}_s$) is 0,7 meters on average, and the average width is 12 meters (Strub-Klein and Sudom, 2012).

Under the sail is the consolidated layer, where the ice blocks is frozen together to form a full layer of ice. The thickness of these shows a large variation from area to area, and have an average thickness (h_{cl}) of 1,6 meters. The thickness is γ distributed and does not vary much along the width of the ridge.

Under the consolidated layer is the keel. The keel is composed of loose rubble and have average depth over the keel ($\bar{h}_k$) and width (w_k) of 4,5 and 36 meters respectively.

The macro porosity (η) can be defined as the relationship between sea water and ice in a ridge, as defined by Shafrova (2007):

$$\eta = \frac{V_{sea\ water}}{V_{sea\ water} + V_{pure\ ice} + V_{brine\ pockets}} \tag{2.6}$$

The average macro porosity of a ridge is found to be 22 %. The sail and keel have on average (η_s) = 18 % and (η_k) = 20 % respectively. The average properties of sea ice ridges found by Strub-Klein and Sudom (2012) is summarized in Table 2.1.

Table 2.1: Dimensions of ice ridges compiled by Strub-Klein and Sudom (2012).

Ice ridge properties			
Sail	max height	$h_{s,max}$	8 m
	average height	$h_{s,avg}$	2 m
	average elevation over sail	$\bar{h}_{s,avg}$	0,7 m
	average width	$w_{s,avg}$	12 m
	average macro porosity	$\eta_{s,avg}$	18 %
Keel	max depth	$h_{k,max}$	28 m
	average depth over keel	$\bar{h}_{k,avg}$	4,5 m
	average width	$w_{k,avg}$	36 m
	average rubble macro porosity	$\eta_{r,avg}$	20 %
Consolidated layer	average thickness	$h_{cl,avg}$	1,6 m

Strub-Klein and Sudom (2012) calculated a series of relationships between different parameters of the ice ridge shapes shown in formulas 2.7a – 2.7b:

$$h_k/h_s = 5,17 \qquad \bar{h}_k/\bar{h}_s = 9,96 \qquad w_k/w_s = 6,75 \tag{2.7a}$$
$$w_s/h_s = 3,75 \qquad w_k/h_k = 4,28 \tag{2.7b}$$

2.3 EM31

The EM31-Mk2-ICE is produced by Geonics Limited, and is an ice specialized version of the EM31-Mk2 instrument, commonly used in geophysical exploration. In this thesis, the EM31-Mk2-ICE will simply be referred to as "EM31". It is constructed with a pair of coils, a transmitter coil (Tx) and a receiver coil (Rx) separated by a distance r = 3,66 m. A sine wave current with a frequency f_{EM} = 9,6kHz is applied to the transmitter coil to generate a varying magnetic field. This field is called the primary field (H_p), and induces an eddy current in the underlying medium. This current again generate a secondary magnetic field (H_s). Both of these fields induces a current in Rx, and the relationship between these two is utilized in order to calculate the sea ice thickness. The coils are mounted in a HCP (horizontal coplanar) configuration. Table 2.2 summarize the specifications of the instrument. A schematic of the application and working of the EM31 is shown in Figure 2.4.

Table 2.2: Specifications of EM31-Ice

EM31-ICE	
Tx-RX distance	r = 3,66 m
Frequency	f_{EM} = 9,6 kHz
Orientation	HCP
Measuring Range	10, 100 and 1000 mS/m
Resolution	$\pm 0,1\%$ of full scale
Accuracy	Conductivity: 0,1 mS/s

The EM31 can be tipped to one of the sides to measure the VCP (vertical coplanar) response. The drawback of using the VCP configuration is that two different depths can give the same results, as described by McNeill (1980). For the EM31 on sea ice, this is a large problem as all the typical sea ice thicknesses are around the tipping point of the response curve. Therefore, only the HCP configuration is covered in this thesis.

2.3.1 Theoretical background

A current $I = I_0 \sin(\omega t)$ is applied to the Tx coil of the instrument to generate an alternating magnetic field. The field generated when current (I) has the maximum value I_0 in free space at Rx is then given by

$$H_p^{Rx} = -\frac{I_0 A}{4\pi r^3} \tag{2.8}$$

where A is the area of Tx. Introducing the homogeneous half-space where a medium with the conductivity σ fills half the space as shown in Figure 2.5, the secondary field due to induced eddy currents in the conducting medium, at Tx then becomes
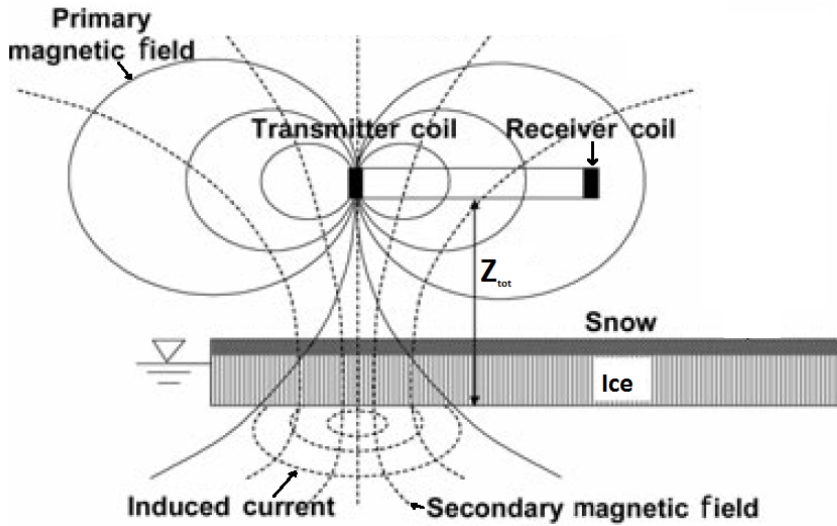
Figure 2.4: Schematic showing the application and working of an EM31 on sea ice. The figure is adapted from Uto et al. (2006).

$$H_s^{Rx} = -\frac{I_0 A}{2\pi r^3}\left[1 - \frac{3}{\phi^2} + [3 + 3\phi + \phi^2]\frac{e^{-\phi}}{\phi^2}\right] \tag{2.9}$$

where ϕ and γ is defined in formula 2.10

$$\phi \equiv r \cdot \gamma, \quad \gamma \equiv \sqrt{i\omega\mu_0\sigma} \tag{2.10}$$

μ_0 is the permeability of free space and $i = \sqrt{-1}$. The ratio of secondary field to primary is then found by dividing the secondary with the primary field, as found by McNeill (1980):
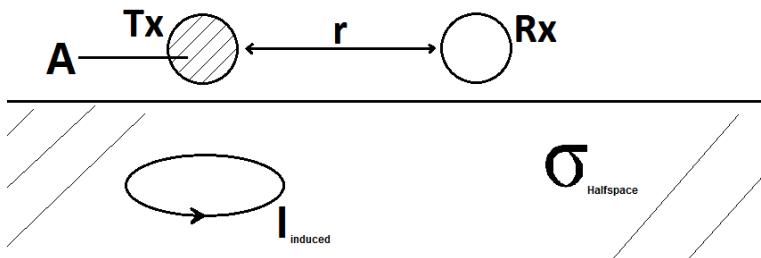
Figure 2.5: Diagram showing the EM31 in a homogeneous half-space. The EM31 is shown in vertical coplanar configuration to keep the diagram simple.

$$\left(\frac{H_s}{H_p}\right)^{Rx}_{HCP} = 2\left[1 - \frac{3}{\phi^2} + [3 + 3\phi + \phi^2]\frac{e^{-\phi}}{\phi^2}\right] \tag{2.11}$$

As can be seen, Equation 2.11 is not trivial, and inverting the equation to extract the conductivity is not possible. Note also that in reality, σ does vary with the depth and makes it even harder to solve. To find an approximation, the induction number is introduced as the separation between the coils divided by the skin depth,

$$B = \frac{r}{\delta} = \frac{\phi}{\sqrt{2i}} = r\sqrt{\frac{\omega\mu_0\sigma}{2}} \tag{2.12}$$

where the δ is the skin depth, defined in Equation 2.13. The skin depth is the depth at which point the primary field is reduced by a factor of $1/e$.

$$\delta = \frac{\sqrt{2i}}{\gamma} = \sqrt{\frac{2}{\omega\mu_0\sigma}} \tag{2.13}$$

At high induction numbers, the magnetic field at Rx is only from the primary field transmitted through free space, as the field going into the conducting medium is completely attenuated. At low induction numbers both fields reach Rx. If it is assumed that the instrument is working at low induction numbers ($B \ll 1$), Equation 2.11 can be simplified to

$$\left(\frac{H_s}{H_p}\right)^{Rx}_{HCP} \approx \frac{iB^2}{2} = \frac{i\omega\mu_0\sigma r^2}{4} \tag{2.14}$$

This is known as the small numbers approximation. To fulfill this requirement, the following must hold

$$\sigma \ll \frac{2}{\mu_0\omega r^2} = 1,9697 \ \frac{S}{m} \tag{2.15}$$

As ω and r is fixed in the EM31, the maximum mean conductivity measured by the EM31 under the small numbers approximation is significantly less than the common conductivity of sea water ($\sigma_{SW} \approx 2,2 - 2,8 \ S/m$). For thin ice and open water, this approximation does not hold. Assuming that the approximation holds, the conductivity the EM31 senses can be found by using the quadrature component of the sensed magnetic field, as shown below.

$$\sigma_a \equiv \frac{4}{\mu_0\omega r^2}Im(\frac{H_s}{H_p}) \qquad \left[\frac{S}{m}\right] \tag{2.16}$$

where σ_a is the apparent conductivity sensed by the EM31. This Equation is built into the EM31 and is the primary output of the system. Note that this formula gives the σ_a in SI-units, and not in millisimens per meter as used in the calculations. This Equation is first

defined by McNeill (1980), and used by Haas et al. (1997), Uto et al. (2006), Tateyama et al. (2006) and more.

It is important not to misuse the apparent conductivity, and such misinterpret the response and make false assumptions. A comprehensive review of this subject is given in Spies and Eggers (1986), where they discuss the apparent resistivity. Apparent resistivity is the inverse of the apparent conductivity, $\rho_a = 1/\sigma_a$.

2.3.2 Cumulative response

A simple method of calculating the response of the EM31 at a given structured halfspace is to use the relative response (Φ) of the different depths to the measured apparent conductivities as formulated by McNeill (1980). The relative response is the amount each layer contributes to magnetic field,

$$\Phi_H(\lambda) = 2 - \frac{4\lambda}{\sqrt{4\lambda^2 + 1}} \tag{2.17}$$

where λ is the normalised depth, $\lambda = Z/r$, where Z is the actual depth in meters. If the relative response is integrated from the normalized depth to infinity, the cumulative response (R) is found. The cumulative response can be interpret as the response of all that is at depth λ and downwards.

$$R_H(\lambda) \equiv \int\limits_{\lambda}^{\infty} \Phi_H(Z)d\lambda = \sqrt{4\lambda^2 + 1} - 2\lambda \tag{2.18}$$

Calculating the apparent conductivity sensed by the EM31 can then be found using equations 2.19a - 2.19d shown in Figure 2.6:

$$\sigma_{a,1} = \sigma_1 \tag{2.19a}$$
$$\sigma_{a,2} = \sigma_1[1 - R_1] + \sigma_2 R_1 \tag{2.19b}$$
$$\sigma_{a,3} = \sigma_1[1 - R_1] + \sigma_2[R_1 - R_2] + \sigma_3 R_2 \tag{2.19c}$$
$$\vdots \qquad\qquad \vdots$$
$$\sigma_{a,n} = \sigma_1[1 - R_1] + \left(\sum_{i=2}^{n-1} \sigma_i[R_{i-1} - R_i]\right) + \sigma_n R_{n-1} \tag{2.19d}$$

where $R_i = R_H(\lambda_i)$ and $\sigma_{a,n}$ is the apparent conductivity measured by the instrument at a n-layer model. Inverting equation 2.19 with regards to R_{n-1} of the bottom layer, it is quite clear that only the two layer-, and possible the three layer (if the snow thickness is
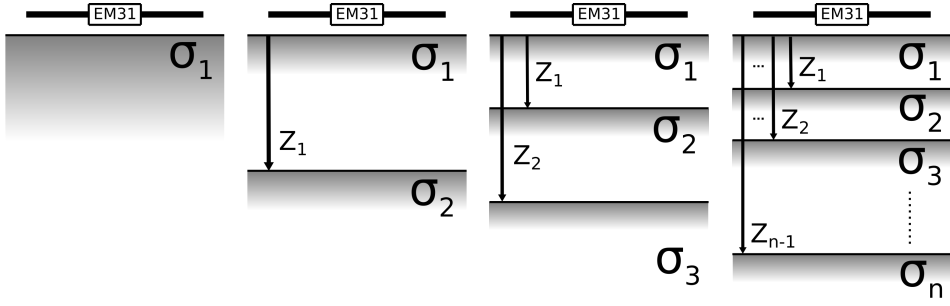
Figure 2.6: Cumulative response from increasing number of layers, i = 1, 2, 3 and n.

measured) model is of any practical use for determining the sea ice thickness, as shown in equation 2.20:

$$R_1(\sigma_{a,2}) = \frac{\sigma_{a,2} - \sigma_1}{\sigma_2 - \sigma_1} \tag{2.20a}$$

$$R_2(\sigma_{a,3}) = \frac{\sigma_{a,3} - \sigma_1[1 - R_1] - \sigma_2 R_1}{\sigma_3 - \sigma_2} \tag{2.20b}$$

$$R_3(\sigma_{a,3}) = \frac{\sigma_{a,3} - \sigma_1[1 - R_1] - \sigma_2[R_1 - R_2] - \sigma_3 R_2}{\sigma_4 - \sigma_3} \tag{2.20c}$$

$$\vdots \qquad\qquad \vdots$$

$$R_{n-1}(\sigma_{a,n}) = \frac{\sigma_{a,n} - \sigma_1[1 - R_1] - (\sum_{i=2}^{n-2} \sigma_i[R_{i-1} - R_i]) - \sigma_{n-1} R_{n-2}}{\sigma_n - \sigma_{n-1}} \tag{2.20d}$$

These equations is a simplification of the real response, but can give some pointers to the expected response.

2.3.3 Experimental

To find the experimental relationship between the sea ice thickness and the apparent conductivity, one have to measure the thickness of the ice by using ice thickness drilling, and at the same spot read the EM31 response. It is important to measure the EM31 reading before the bore is made, as the sea water in the bore will affect the reading. The most significant work on this is Haas et al. (1997), where they compiled three separate equations for winter (σ_{a_w}) , summer (σ_{a_s}) and for the year average (σ_{a_y}) given in equations 2.21a - 2.21c.

$$\sigma_{a_w} = 95.8 + 1095.5 \exp(-0.995 Z_{I_w}) \tag{2.21a}$$

$$\sigma_{a_s} = 57.2 + 1270.9 \exp(-0.900 Z_{I_s}) \tag{2.21b}$$

$$\sigma_{a_y} = 62.5 + 1273.9 \exp(-0.915 Z_{I_y}) \tag{2.21c}$$

where Z_{I_x} is the measured ice thickness from drilling. Haas et al. (1997) then inverts the equations and get the equations for ice thickness as a function of the apparent conductivity (Equations 2.22a - 2.22c):

$$Z_{a_w} = 7.03 - \ln(\sigma_{a_w} - 95.8)/0.995 \tag{2.22a}$$
$$Z_{a_s} = 7.94 - \ln(\sigma_{a_w} - 57.2)/0.900 \tag{2.22b}$$
$$Z_{a_y} = 7.81 - \ln(\sigma_{a_w} - 62.5)/0.915 \tag{2.22c}$$

The general form of these equations in Haas et al. (1997) is then (equation 2.23):

$$\sigma_a(Z_I) = C_1 + C_2 \cdot \exp(-C_3 \cdot Z_I) \tag{2.23a}$$
$$Z_I(\sigma_a) = D_1 - \ln(\sigma_a - D_2)/D_3 \tag{2.23b}$$

where C_x and D_x are constants. This form is also used by Haas (1998), Tateyama et al. (2004) and Eicken (2009). There are other exponential forms used by Reid et al. (2006a) and Tateyama et al. (2004).

2.4 CTD

A CTD is an oceanographic instrument that measures the conductivity (C), temperature (T) and depth (D) as it is lowered down into the water. These values are then used to derive the salinity, temperature and density of the water masses. The conductivity node of the CTD is built such that the water passes between two to four non-corrosive metal nodes connected to a measuring circuit. The Pressure sensor is usually a strain gauge (Wells, 2011). The CTDs used in this work have all been from SeaBird Inc. and have good accuracy for the conductivity and depth.

Method

The Method section in this thesis is divided into four parts, *Techniques (3.1)* where the field techniques and instrumentation is presented, *Field locations (3.2)*, *Fieldwork (3.3)* where fieldwork in it self is presented. Lastly the *Simulation and programming (3.4)* is presented.

3.1 Techniques

The field techniques applied in the work do for the most part follow the standard set by Eicken (2009). It will nonetheless be described in detail, as even small deviation can have great effect on the result.

3.1.1 Ice core

The ice cores were taken using a glass fibre ice core bore, and following the procedure outlined in Eicken (2009). First, the temperature was measured at 10 cm intervals. Then the core was cut into around 10 cm long pieces and put into boxes, then later melted to measure salinity.

3.1.2 Ice thickness Drilling

The ice thickness drilling is done by drilling a narrow hole with either a narrow (approx 5cm diameter) bore or a thicker (approx 25 cm diameter) bore. The bore diameter does not influence the measured thickness, and is decided based on which equipment that was available at the time. Electrical drills was used for the narrow bore and a gas driven drill was used for the thick bore. The advantage with the electrical drills is that it works with

little or no problem, the disadvantage is the battery life. The gas driven drill is much more powerful, and needed 2 persons to operate. The snow layer on top where also measured at the same time using a common ruler.

The measurements where taken by a metal ruler with a end bent in a L shape. During the drilling on the ridge a ruler was placed next to the drill to find pockets where the drill fell. This was unnecessary as there where no noticeable pockets in the ridge.

3.1.3   EM31 Sounding

The use of the EM31 to measure ice thickness in either automatic continuously mode or in station-by-station mode. In the automatic mode, the instrument take measurements at every second, noting the GPS position, the quadrature and in-phase component and calculates the ice thickness using an in-built method. This method makes it possible to measure large areas with little extra work. The station-by-station measurements is done by manually reading the EM31-output quadrature component at each station. This method is more suited for exact reading in for example a grid. When measuring, it is normal to either carry the EM31, drag it on a sledge (pulka), or put it down on the ice for each station.

3.2   Field locations

The fieldwork of this thesis has been done in and around the Svalbard archipelago during the spring of 2014. Svalbard is an ideal location for studying sea ice, as there is a good infrastructure, and the ice edge is going along the Svalbard archipelago. The west coast is mostly free from ice during the winter, with exception of the fjords, due to the Svalbard Branch (SB) of the West Spitsbergen Current (WSC) bringing warm water from the south (Piechura and Walczowski, 2009). The WSC is the northern part of the North Atlantic Current (NAC). The east side of Svalbard is mostly covered by ice during the winter and spring.

The work has been divided between four different locations at Svalbard shown in Figure 3.1. Longyearbyen (1) where UNIS is located, Svea (2 and 3) for testing on level ice, Dunérbukta (4) for some field-testing, and Storfjorden (5) where the ice ridge and ice floe[1] was measured.

3.2.1   Svea

Svea is located in the inner part of Van Miljefjorden (Figure 3.2), and is the location of the largest coal mine on Spitsbergen. The fjord is often covered by ice due to Axeløya blocking the inlet, and is divided in an outer and inner basin. It has been a field site for the Technology group at UNIS for a long time (Høyland, 2009). Two sites at Svea have been

---

[1] **Floe:** *Any relatively flat piece of sea ice 20 m or more across* (WMO, 2009)

measured, the ice outside of Kapp Amsterdam (1) and the ice in Sveasundet (2), during the fieldwork from March 30 to April 3, 2014.

Kapp Amsterdam

Kapp Amsterdam is the port of Svea, capable of receiving large coal ships. The fieldwork was done on the ice at the south side of the port. The ice was almost completely level, as shown in the 20m Synthetic aperture radar (SAR) image (Figure 3.3a), and in picture of Kapp Amsterdam (Figure 3.3b). There was some wind packed snow on top of the ice, varying between 5 and 20 cm. A 7 x 7 calibration grid has been made and measured with drilling and EM31.

Sveasundet

Sveasundet is the strait between Sveabukta and Braganzavågen and is at the most narrow point 694 meters across. The ice here was also flat. A transect across the strait, carrying the EM31 and drilling holes every 20-30 meters. The main purposes of this transect was to ensure the safety of the Bandwagon driving over the strait to pick up supplies. However, the data will be used as a calibration and test of the EM31 as both EM31 and manual measurements have been collected.

3.2.2   Storfjorden

Storfjorden is the fjord between Spitsbergen and Edgeøya – Barentsøya (Figure 3.1, #5). Storfjorden can even in summer be full of drift ice (Jaklin, 2003), and is therefore an ideal place to look for drift ice during winter, when the ice pack is even greater. The ship used was the RV Lance from the Norwegian Polar Institute. The plan was to go through Freemansundet and into Olgastretet, then further up towards Hinlopenstretet looking for a suitable ice floe. When we were emerging from Freemansundet it was clear that the ice condition on the east side of Barentsøya was insufficient. Consequently it was decided to head back to Storfjorden where the conditions was looking better, as can be seen in Figure 3.4. Back in Storfjorden we found a suitable floe outside of Mohnbukta, inside the circle in Figure 3.4a, where we moored into the floe. The ice floe was approximately 500x1000 meters with a flat ice area close to the ship, an iceberg frozen in that was approximately 11 meters thick, and a small ice ridge. During the stay the icefloe drifted freely southwards as can be seen in Figure 3.4b. As the floe drifted southward it also rotated, as also can be seen in the figure.

3.2.3   Dunérbukta

Dunérbukta is located on the west side of Spitsbergen (Figure 3.1, #4), going out into Storfjorden. It is quite shallow, only around 17 meters and Ulvebreen glacier is calving out into the bay. The fieldwork done in Dunérbukta was done as a part of the course 'AGF311
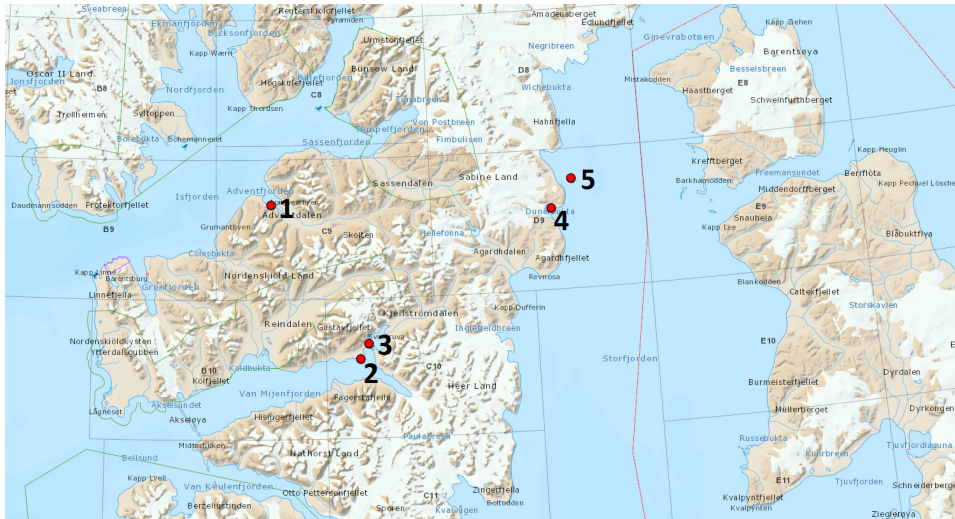
Figure 3.1: Map of Svalbard showing the five different locations. 1) Longyearbyen, 2) Kapp Amsterdam, 3) Sveasundet, 4) Dunérbukta and 5) Storfjorden. Map by courtesy of the Norwegian Polar Institute (2015)
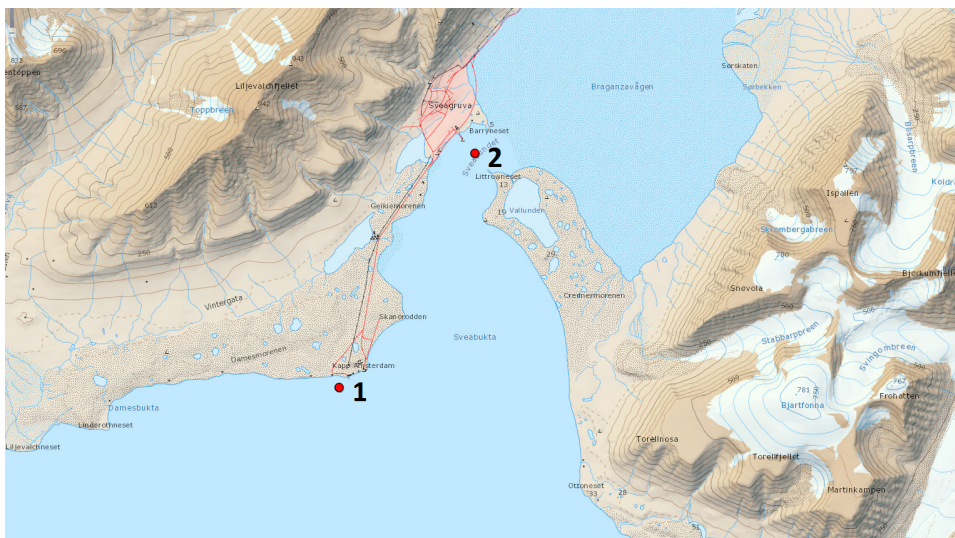
Figure 3.2: Map of Svea showing the two field sites 1) Kapp Amsterdam and 2) Sveasundet. Map by courtesy of the Norwegian Polar Institute (2015).

(a) SAR Image (b) Kapp Amsterdam
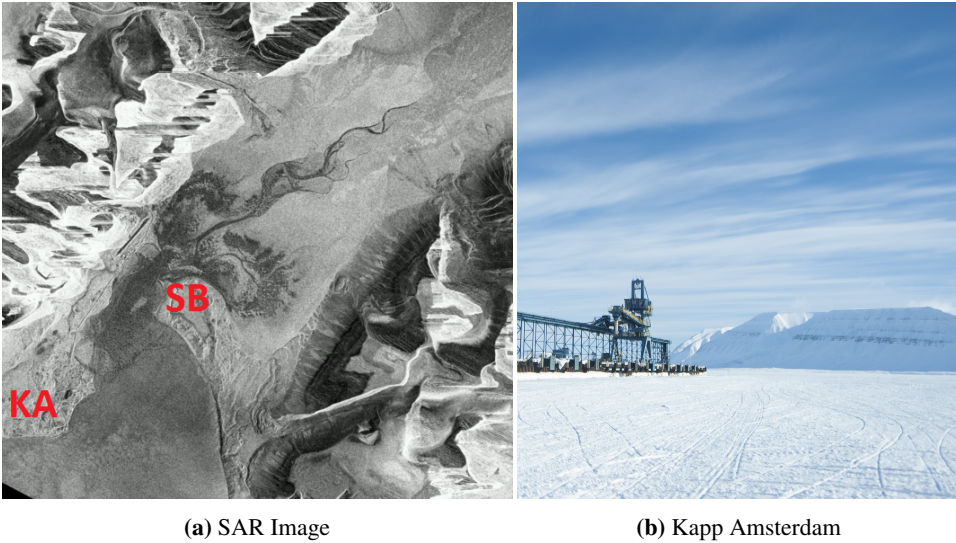
Figure 3.3: a) SAR image of Svea taken 9th March 2014 by ENVISAT, that indicates that the sea ice around Kapp Amsterdam and Sveasundet is flat. SB: Svea- bukta, KA: Kapp Amsterdam. Image by courtesy of Adrian Lockman at the 'Calving Rates and Impact on Sea Level' (CRIOS) project. **b)** Photo of the Kapp Amsterdam taken at 31th of March 2014.
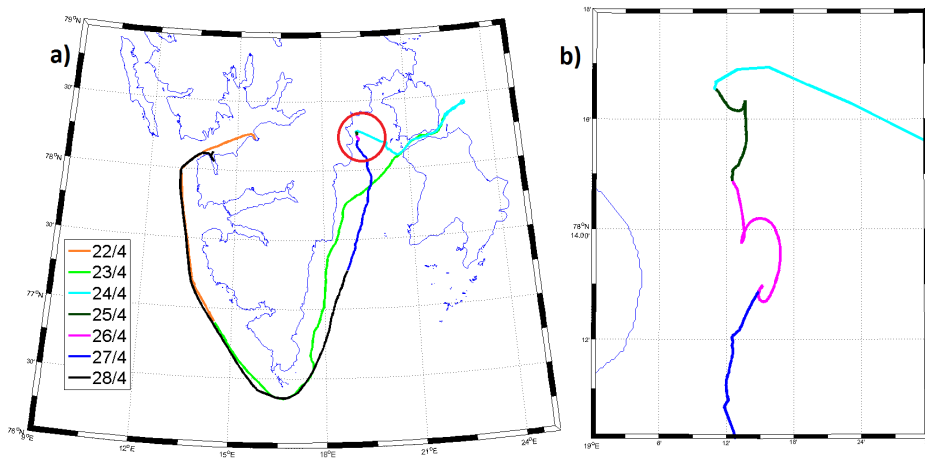
Figure 3.4: GPS Track of RV Lance from 22th to 28th of April 2014. a) The full track, the circle indicates the moored location in b). b) Tack of the ship while moored to the ice floe. The rotating pattern is due to the drift of the floe.

- Remote Sensing of the Cryosphere' at UNIS, and the work is therefore reduced to testing of the equipment and further data to test the models. It was done a small 5 by 6 measuring grid with the EM31-ICE and some simple testing with the echo sounder.

3.3 Fieldwork

The fieldwork is summarized in Table 3.1, showing the main activities at each site. The iceberg in Storfjorden was measured with the echo sounder, and this is discussed in Appendix A. In total 15 days in field, including the entire cruise at three different locations. In this section, the fieldwork is divided into two parts, level ice and the ice ridge.

Table 3.1: Overview of Fieldwork Spring 2014

Fieldwork Spring 2014		
	Date	Data
Dunérbukta	19/03 – 19/03	• Level ice grid • Ice core
Svea	29/03 – 04/04	• Level ice grid • Long section • Ice core[2]
Storfjorden	22/04 – 29/04	• Ice Ride • Level Ice • Ice berg[3]

As most of the work was conducted in cooperation with students from the course "AT-211 Ice Mechanics, Loads on Structures and Instrumentation" at UNIS, much time went to teach the students how to conduct the measurements, in order to ensure a sufficient quality. During the Storfjorden cruise, two of the teachers of the course had to stay back in Longyearbyen, and my teaching responsibilities intensified. I had in periods responsibility for most of the students, at 2-3 different locations on the ice floe. Even as this was immensely educational, it did reduce the time available for the thesis related fieldwork.

3.3.1 Level ice

Dunérbukta

In Dunérbukta, the level ice has been measured by a 5x6 grid with 10 meters spacing, measuring snow depth, ice thickness, freeboard[4] and EM31 thickness. The quadrature

---

[2]Not a standard core, see Section 3.3.1
[3]Discussed in Appendix A
[4]**Freeboard:** *The height of the ice surface above the sea*

component was unfortunately not measured. The automatic ice thickness output of the EM31 was calculated with an sea water conductivity of 2700 mS/m. Ice cores measuring temperature and salinity where also conducted by other students. Ice, snow and working conditions is shown in Figure 3.5.

Figure 3.5: Level ice measured by a 5×6 grid in Dunérbukta. Ice thickness, snow depth, freeboard EM31-thickness has been measured. The automatic thickness where done with $\sigma_{sw} = 2700mS/m$

Svea

In Svea, one 7x6 grid with a spacing of 10 meters, and a transect of 700 meters where measured. The grid where placed next to the port in Kapp Amsterdam and ice thickness, snow thickness, and EM31 measurements where conducted. The EM31 measurements where done carrying the EM31 around the grid, running in automatic and letting the GPS take the position. The transects in Sveasundet where done by first drilling the thickness and marking each hole with a stick on the way over, and then walking with the EM31 on the stretch back. The EM31 could not be put on the sledge of the scooter as it where made of metal. Figure 3.6 shows the two scooters, and the two students helping with the measurements.

Storfjorden

Due to time restraint and lack of manpower, no grid was measured on the ice floe. However on the last day, a group of students where put in charge of pulling the EM31 on a pulka around the ice floe. The pulka was mounted with a rig on which the EM31 was fastened. This lifted the Tx-Rx around 25 cm over the ice. The pulka was then dragged by a student pulling a rope as shown in Figure 3.7. The idea was to walk in a grid pattern, but the students apparently did not fulfill this, as can be seen in Figure 4.6a.

3.3.2 Ice Ridge

The work done at the ice ridge where done by first marking up the grid (Figure 3.9) with sticks as shown in Figure 3.8, then measuring the EM31 response in both broadside and in-

Figure 3.6: Location of the sea ice thickness transect. The picture is taken at the end of the transects, and the two figures are the students of AT-211 helping with the measurements.

Figure 3.7: Student dragging the EM31 around the ice floe during the stay in Storfjorden

line configuration and then drilling the holes, measuring snow thickness and ice thickness. The EM31 was at each station put down to the snow. The effective distance from the ice to the Tx-Rx coils is where then $Z_s + 0.14$m. GPS coordinates and Total Station location where also taken at each point.

Measurements taken at each point at the ice ridge:

- EM31-Ice:
    - In-line ($\sigma_{a,il}$)
    - Broadside ($\sigma_{a,b}$)
- Ice thickness drilling (Z_I)
- Snow thickness (Z_s)
- Total Station Position
- GPS Position

The grid consists of four transects, three crossing the ridge (B–D) and one along the ridge (A). The spacing between the stations is 1 meter for transects B–D and 2 meters for A.

Figure 3.8: The measurements of the ice ridge where done by first marking the grid using sticks, then measuring the EM31 response in both broadside and in-line position and lastly drilling to get the depth of the ice.

Two ice cores where also taken at the ridge. One through the centre of the ridge, and one at the flat area closer to the camera in Figure 3.8.
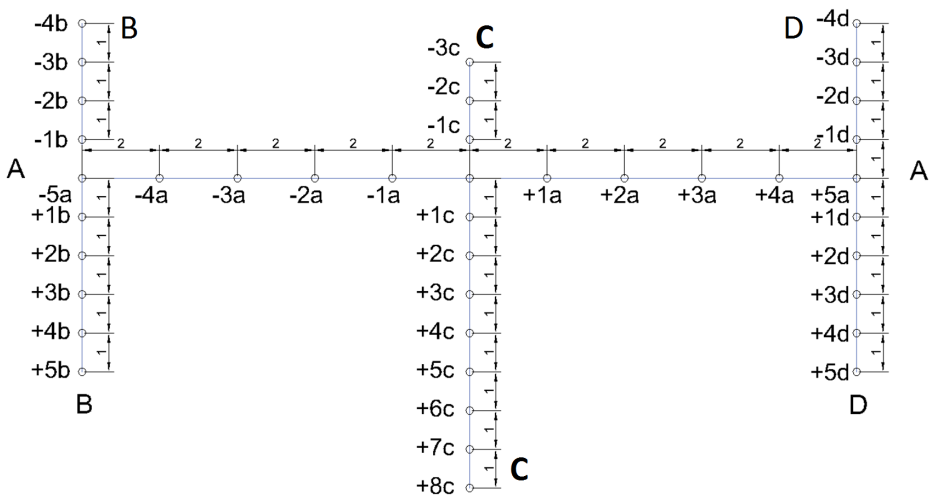
Figure 3.9: Measurement grid for the ice ridge in Storfjorden. The figure is made by the students of AT-211 that worked at the ridge.

3.4 Simulation and programming

3.4.1 Programming languages

All the programming and framework for the simulations have been done using Matlab 2013b. This includes input–output of all other programs, running of other programs and

visualization of the data. The advantage of Matlab is that the production speed of code is quite fast and easy, and that the interface for making graphs and figures are similarly easy (MATLAB, 2013). The interface with the CTD have been written in Phyton 2.7, for making the serial interface more simple to program (Rossum and Drake, 2001).

3.4.2 MarcoAir

The P223 project started in 1980, ended 2008, and had the aim to develop software to model and invert signals from electromagnetic measurements for mineral exploration (Raiche, 2008). All of the programs in the program package have the same interface, but have different capabilities and limitations (Raiche and Sugeng, 2008). The programs have capabilities ranging from simple flat-layered earth (Airbeo) to full 3D domain modelling and inversion (LokiAir). MarcoAir is between these two, having the capabilities to simulate 3D prisms in a flat layer earth host. MarcoAir do however not have the capabilities of inversion as opposed to the rest of the package.

The main reason that MarcoAir has been chosen is that Reid et al. (2003) and Reid et al. (2006a) have used it previous with success simulating simple ice ridges. MarcoAir functions by solving the integrals using a block iterative algorithm with symmetrized integrals as described by Xiong (1992) and Xiong and Tripp (1995).

MarcoAir Interface

The interface of MarcoAir is by text file, and can be quite complex. As this file also needs to be changed for each model run, the generation of the file have been programmed in Matlab. After the file is created and placed in the same folder as the MarcoAir program, MarcoAir is run from terminal, automated with Matlab. The output of MarcoAir is two files, one is a verbose file including the input and output with text describing each parameter. This file is mainly for manual use as a debugging aid. The other file is a compact file made for automatic import and is then imported. This file is then imported into Matlab. In Matlab, a function running MarcoAir for a layered model has been made, as described in algorithm 1.

Algorithm 1 MarcoAir Interface

1: **procedure** RUN MARCOAIR
2:     Create MarcoAir input file
3:     Run MarcoAir
4:     Move output file to data folder
5:     Read output file
6:     Convert to Apparent Conductivity
7: **end procedure**

3.4.3 Deriving experimental $Z(\sigma_a)$ from simulation

The experimental relationship between the thickness of the ice (Z) and the apparent conductivity (σ_a) as calculated in Haas et al. (1997) can also be calculated using electromagnetic simulation. A simple simulation of this kind has been made by Tateyama et al. (2004) and Shirasawa et al. (2006), using the software PCLOOP. PCLOOP was developed by Geonics, as a 1D modelling software. I have used MarcoAir in a flat layered earth without prisms as my simulation tool. The procedure used in the simulation, shown in algorithm 2, can be divided into three parts;

1. Input (pt. 2–3)
2. Modelling (pt. 4–8)
3. Fitting and inversion (pt. 9–11)

Algorithm 2 $Z(\sigma_a)$ from Ice Core

 1: **procedure** $Z(\sigma_a)$
 2:     **Input** Core information [$T(Z)$, $S(Z)$ and Z]
 3:     Calculate $\sigma(Z)$
 4:     **for** $(Z_{tot} = 0, 1...5m)$ **do**
 5:         $\sigma(Z) =$ flatIceScaling
 6:         RunMarcoAir
 7:         Calculate σ_a
 8:     **end for**
 9:     fit $\sigma_a(Z_{tot})$
10:     invert $\sigma_a(Z_{tot}) \rightarrow Z_{tot}(\sigma_a)$
11:     **return** D_n
12: **end procedure**

Input

The input to the simulation is an ice core taken at the site, which include measurements of depth (Z), Temperature (T) and Salinity (S). Then using the method in section 2.1.4, the vertical conductivity profile is calculated. I have used the same m-value as Haas et al. (1997), $m = 1.5$, in these calculations. Further investigation into this value can potentially help the accuracy of the method. These results are then used to compile a conductivity profile of the ice.

Modelling

Then the apparent conductivity is simulated for ice thicknesses Z_{tot} ranging from $0, 1m$ to $5m$. To do this, the ice model needs to be scaled to fit the ice thickness. This can be done in a variety of different ways, and two methods have been implemented. The theory behind scaling of sea ice with regards to electromagnetic properties at low frequency have had little investigation and can benefit from a deeper investigation. The first method of scaling

---

Algorithm 3 flatIceScaling: Even stretch

1: **procedure** EVEN STRETCH
2:     **Input** Z_{tot}, Z_{layers}
3:     $Z_{layers} = Z_{tot} \cdot \frac{Z_{layers}}{|Z_{layers}|}$
4:     **return** Z_{layers}
5: **end procedure**

---

the ice profile implemented is to stretch all layers evenly as formulated in Algorithm 3. This method assumes that the conductivity profile is unaltered by different thicknesses.

The second method implemented is, if Z_{tot} is larger than the total thickness of the ice core (Z_{layers}), to increase the size of the middle layer and keep the thickness of the other layers unaltered. If Z_{tot} is less than the total thickness of the core, then the lowers layers are removed until the core is the right thickness. This method is a bit more complicated than the first as shown in Algorithm 4.

Algorithm 4 flatIceScaling: Layer-wise Scaling

1: **procedure** LAYER-WISE SCALING
2:     **Input** Z_{tot}, Z_{layers}
3:     **if** $sum(Z_{layers}) < Z_{tot}$ **then**
4:         Increase the thickness of the middle layer
5:     **else if** $sum(Z_{layers}[1 : end - 1]) < Z_{tot}$ **then**
6:         **repeat**
7:             Remove bottom layer
8:         **until** $sum(Z_{layers}[1 : end - 1]) < Z_{tot}$
9:         Reduce the thickness of the bottom layer
10:     **else**
11:         Do nothing
12:     **end if**
13:     **return** Z_{layers}
14: **end procedure**

This ice model is then run with MarcoAir, giving the strength of quadrature component of the secondary to primary field ratio ($im[H_s/H_p]$), which is converted to apparent conductivity (σ_a) by formula 2.16, converted to mS/m. Since formula 2.16 is equal to multiply by a constant, no information is lost during this operation. This is done because the EM31 gives σ_a as an output.

Fitting and inversion

After the modelling phase, the apparent conductivity as a function of the ice thickness ($\sigma_a(Z_{tot})$) from the simulation is curve fitted to the form in equation 2.23a using MatLabs internal curve fitting function. MatLabs curve fitting tools also gives the root-mean-square error (RMS) of the curve fit. This exponential function is then inverted to give the desired

function $Z_{tot}(\sigma_a)$ by calculating the coefficients D_1, D_2 and D_3 from C_1, C_2 and C_3 using equations 3.1a – 3.1c.

$$D_1 = \frac{\ln(C_2)}{C_3} \tag{3.1a}$$

$$D_2 = C_1 \tag{3.1b}$$

$$D_3 = C_3 \tag{3.1c}$$

This gives the equation on the form and by the method used by Haas et al. (1997).

3.4.4 Snow compensated Z(σ_a) calculation

One of the advantages of simulation based calculation of the Z(σ_a) equation, is the possibility of using it to compensate for the snow layer. A method of applying this compensation is presented in Algorithm 5. It is done by calculating D_1, D_2 and D_3 for the range of snow depths possible $(0 - 29cm)$ with 1 cm intervals, then an interpolation curve fit (MATLAB (2013), documentation) of the three coefficients. Then for each point, the corresponding formula is calculated from snow thickness and apparent conductivity. The snow layer can for each point be found by interpolating the snow measurements.

Algorithm 5 Snow compensated Z(σ_a) from Ice Core

1: **procedure** Z(σ_a, h)
2:     **Input** Core information [$T(Z)$, $S(Z)$ and Z], σ_a, Snow thickness (Z_{snow})
3:     Calculate ice conductivity $\sigma(Z)$
4:     **for** $= 0...max(Z_{snow})$ **do**
5:         $D_n(h)$ = Calculate Z(σ_a) from $\sigma(Z)$ and h
6:     **end for**
7:     *fit($D_n(h)$)*
8:     Calculate ice thickness for each point using the *fit*, σ_a and Z_{snow}.
9: **end procedure**

3.4.5 Simple level ice modelling of ice ridge

Making a model of an average ice ridge, a simple quasi-2D model of an ice ridge has been simulated by approximate each point as level ice. For each point, the apparent conductivity from both a 12-layer version (n=12) of equation 2.19d ($\sigma_{a,12}$) and level ice simulation using MarcoAir ($\sigma_{a,ma}$). The procedure applied is shown in algorithm 6, where the input is depth of the keel (h_k), the level ice thickness (h_{ice}), the conductivity of the ice (σ_{ice}) and sea water (σ_{sw}), and the macro porosity of the ice ridge keel (η_k).

Model

The model dimensions are calculated from h_k, h_{ice} and η_k using the shape factors and relationships found by Strub-Klein and Sudom (2012) mentioned in section 2.2.1. As the model simulation is quasi-2D, and treat each point as a level ice field, the porosity of the keel can be treated as layers of seawater inside the keel instead of two-dimensional pockets as a full 2D model would require. This overall porosity of the keel can then be split into four layers, as shown in Figure 3.10.

The sail is added as a solid ice block disregarding the macro porosity. The cavities are in reality filled with snow and air, which has a lower conductivity than the ice. An approximation is that these are filled with ice is then reasonable considering the accuracy of the model.

Algorithm 6 Simple level ice modelling of ice ridge

1: **procedure** LEVEL ICE RIDGE MODEL
2:     **Input** $h_k, h_{ice}, \sigma_i, \sigma_{sw}, \eta_k$
3:     Make model
4:     **for** cross section **do**
5:         Calculate $\sigma_{a,12}$
6:         Run MarcoAir $\rightarrow \sigma_{a,ma}$
7:     **end for**
8:     **return** $\sigma_{a,12}(l), \sigma_{a,ma}(l)$
9: **end procedure**
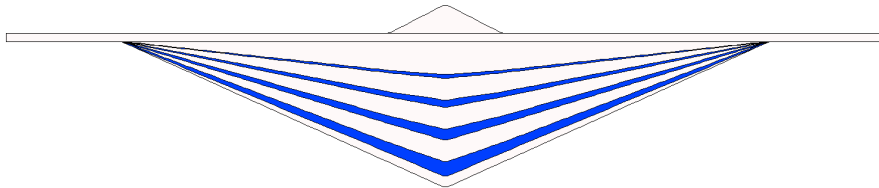
Figure 3.10: Model of an ice ridge with a macro porosity (η_k) of 20%, a sail keel depth (h_k) of 9m and an level ice thickness of 0,5 m. The white areas are the ice, and the blue areas are the sea water intrusion layers.

Chapter 4

Results

The results are divided into four main parts: *Ice cores (4.1)*, where the results of the coring is presented; *Level ice (4.2)*, where all work on level ice is shown; *Ice ridge (4.3)*, where the results from the ice ridge is presented; and *Seawater conductivity (4.4)*.

4.1 Ice cores

In all 8 ice cores are included in this thesis, five in Dunérbukta, one in Svea and two at the ridge in Storfjorden. The results are given in Tables 4.1 and 4.2, and plotted in Figures 4.1 (temperature) and 4.2 (salinity). Of the five cores in Dunérbukta, only Core 2 and 5 were of sufficient quality and length as the core takers were inexperienced. Common for all cores in Dunérbukta was a relatively high temperature at around -1°C. Core 2 shows hints of C-shape in salinity, while Core 5 is closer to an I-shape. In Svea, only one core was taken, and this is technically not a core, but vertical samples through the ice, which is evident by multiple readings at the same depth. Two ice cores taken at the ridge was taken at the centre, close to point C-0 (Core 1) and on the level ice (Core 2). The temperature shows clear linear tendencies, and the salinity can be fitted into the C-shape category.

4.2 Level ice

Three datasets of level ice is presented, a transect from Sveasundet, a 5 by 6 grid taken in Dunérbukta and a EM31 walkabout on the ice floe in Storfjorden. It was, as mentioned, also a 7 times 7 grid measured in Kapp Amsterdam. The EM31 data from this have been corrupted and are therefore omitted.

Table 4.1: Ice cores results in Svea and Dunérbukta

	Dunér. Core 2				Dunér. Core 5				Svea		
L_s	Z	T_i	S_I	L_s	Z	T_i	S_I		Z	T_i	S_I
10	5	-1	5,5	10	5	-1	8,6		3	-10,5	5,61
10	15	-1,5	6,7	10	15	-1,5	3,9		4	-7,8	5,58
10	25	-1	10,2	10	25	-0.6	3,6		4	-9,8	4,96
10	35	-1,7	7,6	10	35	-0.6	3,8		10	-3.8	3,90
10	45	-0,9	5,4	10	45	-0.5	4,5		10	-4,1	4,51
10	55	-1,1	3,6	10	55	-0.5	3,8		14.5	-8,7	3,72
10	65	-0,9	3,2	10	65	-0.6	3,2		20	-9,4	2,92
10	75	-1,2	4,4	10	75	-0.6	3,7		28,5	-7,8	4,72
10	85	-0,7	7,4	10	85	-0.5	4,2		31	-7,0	3,47
-	-	-	-	10	95	-0.8	3,4		-	-	-
-	-	-	-	10	105	-0.8	3,7		-	-	-

Table 4.2: Ice cores taken at the ridge (1) and at the nearby level ice (2)

	Storfjorden Core 1				Storfjorden Core 2		
L_s	Z	T_i	S_I	L_s	Z	T_i	S_I
6.5	3.25	-6.4	9.075	13.0	6.50	-3.3	10.125
9.0	11.00	-5.5	7.605	13.0	19.50	-3.5	5.375
8.0	19.50	-5.4	7.960	13.5	32.75	-3.5	6.530
8.0	27.50	-4.6	5.655	12.7	45.85	-3.1	6.220
10.0	36.50	-4.2	6.435	11.5	57.95	-2.8	9.110
9.5	46.25	-4.0	6.570	11.0	69.20	-2.6	9.459
10.5	56.25	-3.8	5.160	11.5	80.45	-2.6	8.070
11.5	67.25	-2.9	5.745	9.0	90.70	-2.6	7.053
9.0	77.50	-2.5	7.425	-	-	-	-
8.0	86.00	-2.1	6.140	-	-	-	-
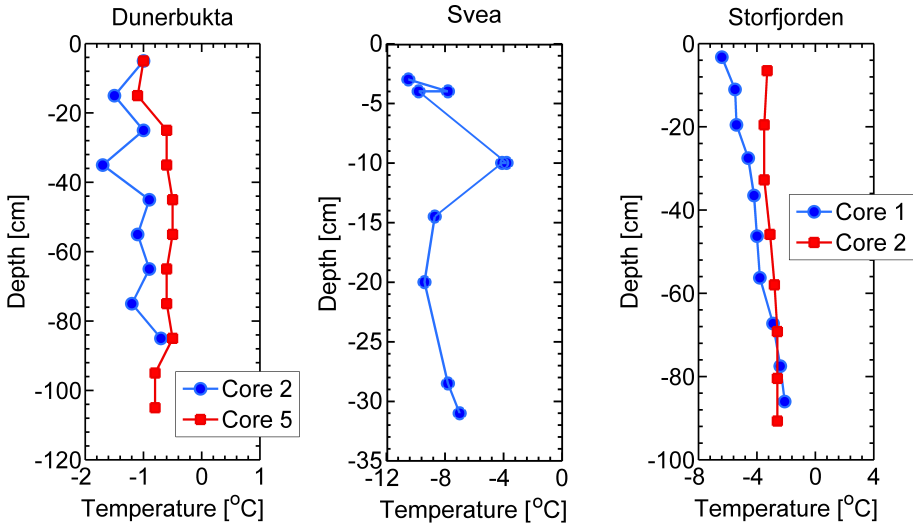
Figure 4.1: Temperature profiles from the cores in Dunérbukta, Svea and Storfjorden. In Dunér-bukta, only Core 2 and 5 are shown. Note that the depth scale is different for each location
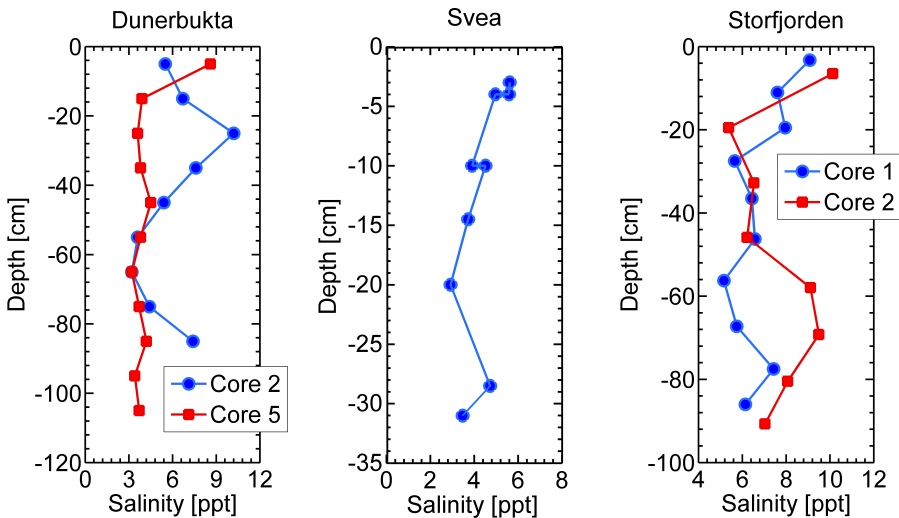
Figure 4.2: Salinity profiles from the cores in Dunérbukta, Svea and Storfjorden. In Dunérbukta, only Core 2 and 5 are shown. Note that the depth scale is different for each location.

4.2.1 Sveasundet

The transect over Sveasundet measured first snow and ice thickness, and then the EM31 was carried on the way back. The carry height was 98cm. Figure 4.3 is a visualization of the ice and snow layers on the transect. The gray area is the snow layer and the light blue is the ice from drilling. The thickness scale is calculated with the assumption that the ice has an density of 0,9. The stations are approximately 30 meters apart. In station 17 and 18, dirt was found, indicating that this area was either grounded or nearly grounded. In Figure 4.4 the apparent conduc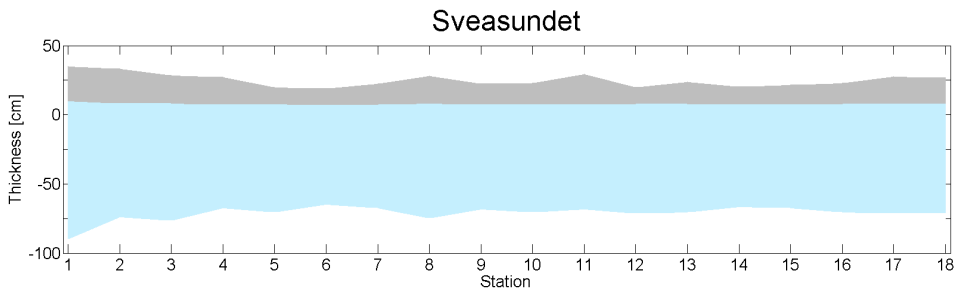tivity and the calculated ice thickness from the built in software are presented. Both show a relative flat profile, with a fall (and rise for the thickness) at the end, in the area where the ice possibly was grounded. The average conductivity on the main part is around 325 mS/s, and the average thickness on the same stretch is around 1,75m.

Figure 4.3: Ice and snow thickness measured as a cross section over Sveasundet. The blue part is the ice, and the gray is the snow. The figure is calculated assuming an ice density of 0,9. Holes 17 and 18 showed dirt when drilled, indicating that the ice was grounded.

4.2.2 Dunérbukta

The 5 by 6 grid in Dunérbukta is presented in Figure 4.5. The grid is interpolated and plotted as an contour plot showing the different values, for ice and snow thickness, freeboard and apparent conductivity. The X and Y axis shows the distance and each tick shown is corresponding with the grid, with 10 m spacing. As can be seen, the ice thickness varies between 0,5 and 1 meters, the snow thickness is between 0 and 30 cm, and most of the freeboard is negative, down to -24,6 cm at one point. The conductivity varies between 400 and 700 mS/m.
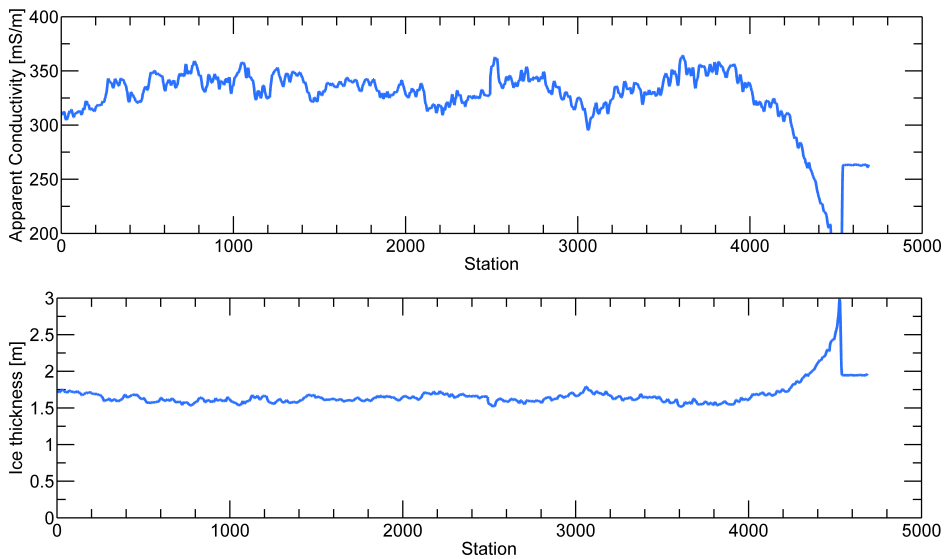
Figure 4.4: Measured apparent conductivity and calculated thickness using the built in software over the Sveasundet transect. During the end of the transect, drilled holes showed that the ice was grounded. The instrument where carried at 98cm. Station refer to the measurements number from the EM31.
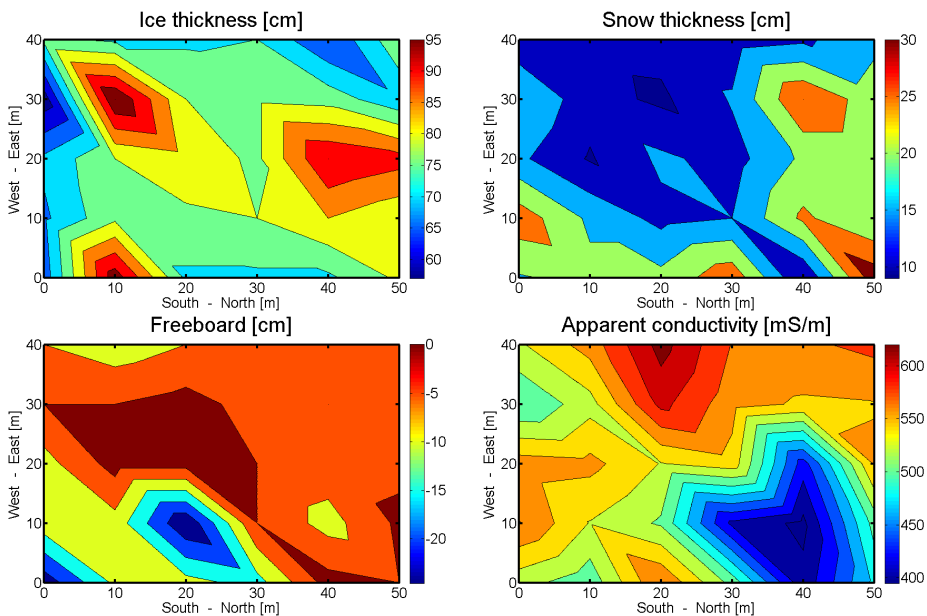
Figure 4.5: The 5 by 6 ice grid in Dunérbukta. From the top left, drilled thickness, snow depth, freeboard and apparent conductivity. The data is interpolated and plotted. The ticks on the axis corresponds to the measured grid, with a 10 m spacing between each point. Note that the scale on the freeboard is negative.

4.2.3   Storfjorden - Walkabout

The EM31 Walkabout conducted on the last day on the ice floe is shown in Figure 4.6. In Figure 4.6a, the calculated ice thickness from the built in software ($\sigma_{sw} = 2700$ mS/m) is interpolated inside the convex hull and plotted. This gives rise to some interpolation effects, like the bleeding in the top corner. The thicker areas close to the stern is an area with thick snow. The red line is the path the students dragged the EM31. Figure 4.6b shows the interpolated apparent conductivity map of the region. The apparent conductivity ranges from 480 to 650 mS/m.

4.3   Ice ridge

The measurements taken at the ice ridge is shown in Table 4.3 after the grid defined in Figure 3.9. Z_d is the drilled ice thickness and Z_s is the snow thickness, both in cm. Two directions of the instrument is measured, the Tx-Rx axis perpendicular ($\sigma_{a,\perp}$) and parallel ($\sigma_{a,||}$) to the ridge direction are given in mS/m. All the readings from the EM31 are taken when the instrument is standing horizontally at the ice, whenever it was possible. Places where the instrument could not be placed on the ice are omitted. The maximum thickness from the drilling is 170 cm and the minimum is 32 cm, and the maximum snow thickness was 45 cm. The measured snow and ice thickness values are visualized in Figure 4.7, calculated with an assumed ice density of 0,9. The blue and grey areas is the ice and snow respectively.

4.4   Seawater conductivity

The sea water conductivity measured in Dunérbukta was 500 mS/m, which is drastically different from the expected result of more than 2000 mS/m. In Svea, the instrument froze, so there is no measurements. In Storfjorden, the CTD measured a conductivity of 2734 mS/m.
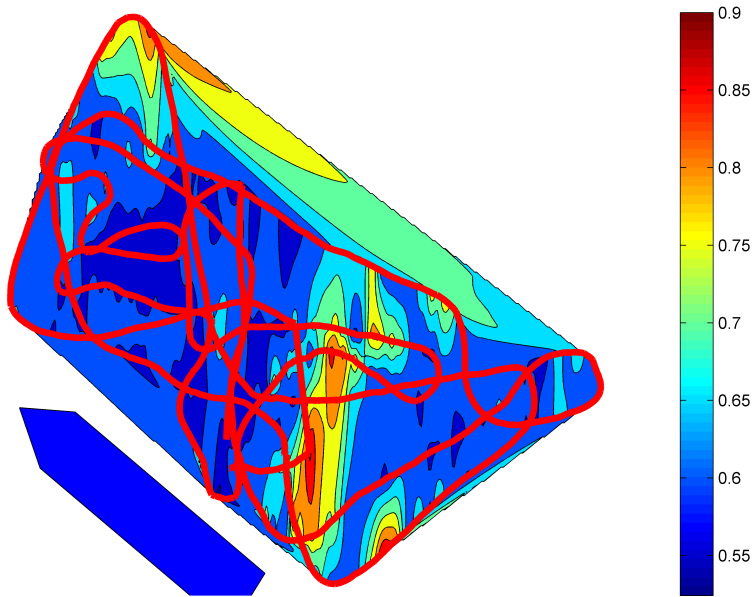
(a) Ice thickness [m]. The thickness is calculated using the built-in automatic calculation with $\sigma_{sw} = 2700$ mS/m. The red line is the path the EM31 was dragged.
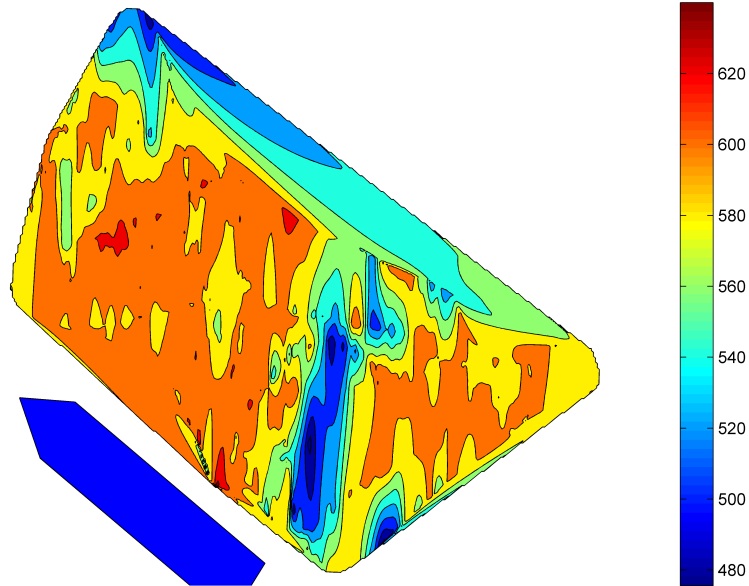
(b) Apparent conductivity (σ_a), [mS/m].

Figure 4.6: EM31-Walkabout in Storfjorden. The blue figure to the left is RV Lance, with length of 61m and width of 13m.

Table 4.3: Results from the ice ridge as measured at the 26th of April 2014 in Storfjorden. The sections corresponds to the grid shown in Figure 3.9. Points AB, AC and AD are the overlapping points from sections B, C, D. Z_d, Z_s is the drilled and snow thickness respectively, $\sigma_{a,||}$ and $\sigma_{a,\perp}$ is the parallel and the normal measurements of apparent conductivity.

Section: A						Section: C					
Tran.	#	Z_d	Z_s	$\sigma_{a,||}$	$\sigma_{a,\perp}$	Tran.	#	Z_d	Z_s	$\sigma_{a,||}$	$\sigma_{a,\perp}$
AB	-5	190	5	504,00	466,00	C	-3	55	20	609,00	541,50
A	-4	180	16	492,25	577,00	C	-2	55	30	528,25	464,75
A	-3	150	12	483,25	576,25	C	-1	120	35	397,75	-
A	-2	120	10	485,50	575,00	C	+1	110	-	453,25	-
A	-1	110	5	453,00	530,50	C	+2	65	-	559,25	-
AC	0	140	20	374,50	349,75	C	+3	65	1	630,75	575,25
A	+1	170	45	387,00	454,00	C	+4	65	1	644,75	595,25
A	+2	110	28	391,00	482,00	C	+5	65	1	648,50	644,25
A	+3	110	2	341,00	521,00	C	+6	65	1	649,50	646,50
A	+4	100	26	-	-	C	+7	65	1	655,50	654,50
AD	+5	105	15	-	-	C	+8	65	1	654,50	670,00

Section: B						Section: D					
Tran.	#	Z_d	Z_s	$\sigma_{a,||}$	$\sigma_{a,\perp}$	Tran.	#	Z_d	Z_s	$\sigma_{a,||}$	$\sigma_{a,\perp}$
B	-4	51	-	690,00	616,00	D	-4	39	-	597,00	610,00
B	-3	51	-	715,00	589,00	D	-3	35	-	640,00	560,00
B	-2	53	-	658,00	545,00	D	-2	32	-	640,00	531,00
B	-1	66	-	505,00	515,00	D	-1	58	-	520,00	525,00
B	+1	120	-	394,00	541,00	D	+1	75	-	512,00	583,00
B	+2	90	-	508,00	512,00	D	+2	65	-	590,00	590,00
B	+3	68	-	588,00	537,00	D	+3	56	-	640,00	589,00
B	+4	58	-	630,00	677,00	D	+4	55	-	660,00	627,00
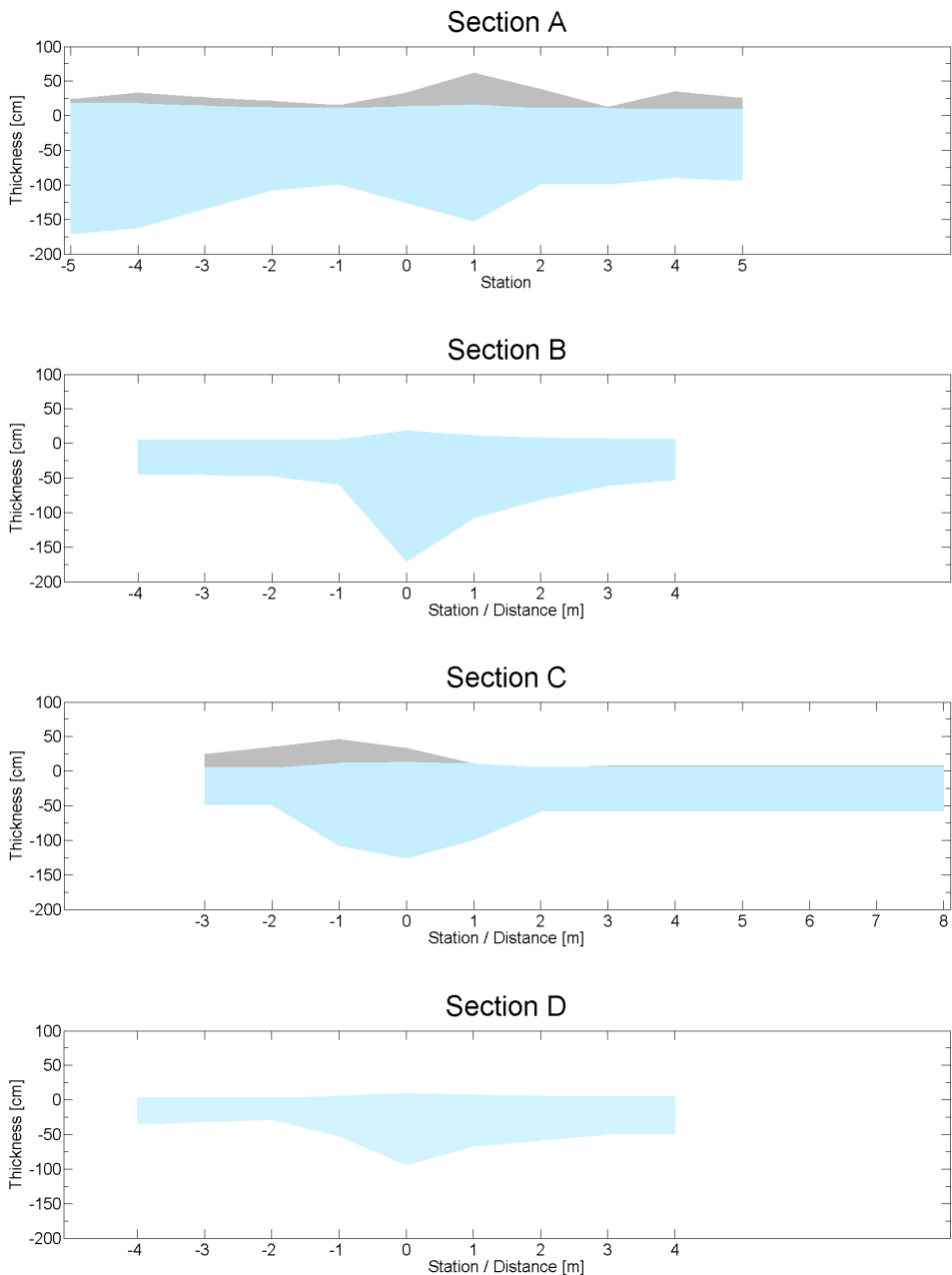
Figure 4.7: Snow and ice thickness measured at the ice ridge during the stay in Storfjorden when drilling. The blue is the ice and the grey is the snow layer. Section A is the section along the top of the ridge, and has a spacing of 2m between each point. Section B, C and D is cross section with a spacing of 1 meter between each point. The figure is calculated assuming an ice density of 0.9.

Chapter 5

Simulation results and analysis

5.1 Calculation of $Z(\sigma_a)$ coefficients

The first step in simulating the EM31 response and find the $Z(\sigma_a)$ coefficients is to calculate the conductivity profiles. Using Archies Law (Equation 2.3) the conductivity profiles of the five cores has been calculated from the temperature and salinity profiles. They are shown in Figure 5.1, and they are somewhat different. The conductivities in Dunérbukta is much higher than Storfjorden, and this is much higher than in Svea. These three different regions will give an good estimate of the variability of the simulation.

5.1.1 Simulation

The simulation is run according to Algorithm 2, for all five profiles using the corresponding sea water conductivity. In Svea where the CTD froze, $\sigma_{sw} = 2700mS/m$ was used in stead, as this is the standard setting of the instruments. The conductivity of the water masses is most probably lower than that, due to the large influx of fresh water. In Dunérbukta, the $\sigma_{sw} = 500mS/m$ measured by the CTD was used. As this appears to be an error, the coefficients have also been calculated with an seawater conductivity of $\sigma_{sw} = 2700mS/m$. All the coefficients have been calculated using an instrument height of 0,14 meters. In Table 5.1, the coefficients from Haas et al. (1997) also have been included as a comparison. The ice is scaled according to Algorithm 3, where the conductivity profile is stretched evenly. The influence of the scaling algorithm is discussed later in this section. The root-mean-square error (RMS) of the Equation 2.23a curve fit is also calculated.

   The results of the simulation, fit and inversion shown in Table 5.1 and plotted in Figure 5.2, shows a clear difference between the three sites. The calculated response in Dunérbukta, when $\sigma_{sw} = 500mS/m$, is as expected drastically different from the other results.
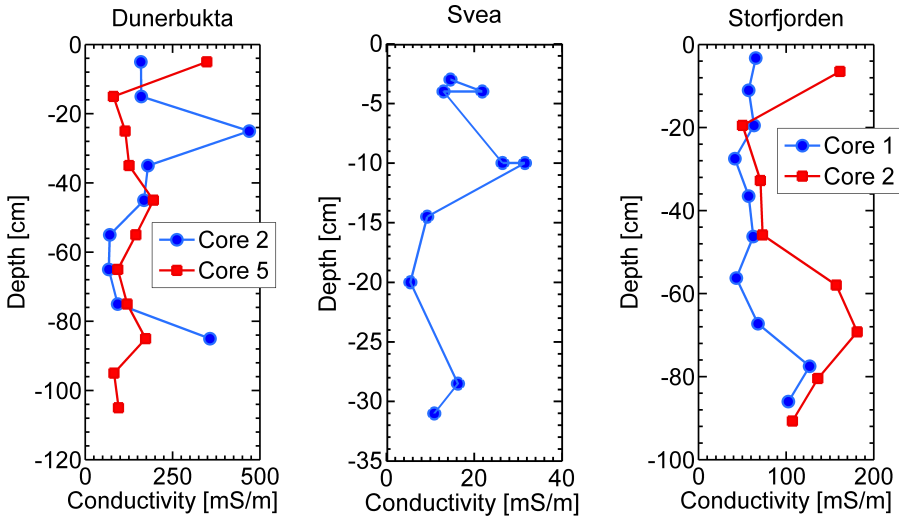
Figure 5.1: Conductivity profiles calculated using Archies Law (Equation 2.3). In all 5 profiles have been calculated, two from Dunérbukta, one from Svea and two from Storfjorden. Note that the depth scale is different for each location

Table 5.1: Coefficients for $Z(\sigma_a)$ calculated from simulation with MarcoAir, conductivity profiles from ice core and conductivity of the water masses below from the CTD. In Svea, there was no CTD data, and $\sigma_{sw} = 2700 mS/m$ have been used. In Dunérbukta, where the results from the CTD was 500 mS/m, the coefficients have also been calculated with $\sigma_{sw} = 2700 mS/m$, marked with a "*". All coefficients have been calculated for an instrument height of 0,14 meters, and with the even stretch algorithm.

		C_1	C_2	C_3	RMS	D_1	D_2	D_3
Level ice fit coefficients calculated from conductivity								
Dunérbukta	Core 2	159,4	182,4	0,810	0,0173	6,43	159,4	0,810
	Core 5	144,8	203,2	0,941	0,1363	5,65	144,8	0,941
	Core 2*	154,3	975,5	0,909	0,0253	7,58	154,9	0,909
	Core 5*	141,8	993,7	0,927	0,0397	7,45	141,8	0,927
Svea		36,5	1087,1	0,849	0,0197	8,24	36,5	0,849
Storfjorden	Core 1	63,2	1069,3	0,857	0,0209	8,13	63,2	0,857
	Core 2	95,6	1040,2	0,876	0,0252	7,93	95,6	0,876
Haas et al. (1997)	Winter	95,8	1095,5	0,995	-	7,03	95,8	0,995
	Summer	57,2	1270,9	0,900	-	7,94	57,2	0,900
	Year	62,5	1273,9	0,915	-	7,81	62,5	0,915

All of the results are reaching an asymptote at between 3-5 meters ice thickness. The asymptote is approximately the mean conductivity of the ice layer, as corresponds to an infinite thick ice layer. The sensitivity to ice thickness change is therefore also reduced when the ice become thicker. At more than 4 meters thickness, the instrument is for all practical purpose not able to differentiate between thicknesses. It can be seen that the ability to determine difference in ice thickness is dependent on two factors,

a) The sea water conductivity σ_{sw}
b) The average ice conductivity $\bar{\sigma}_I$

where the sea water conductivity mostly influences the sensitivity when measuring thinner ice, and the average ice conductivity influences the maximal ice thickness for the instrument. Note that at a very thick level ice, the instruments sensitivity can be increased, improving the measurements somewhat.
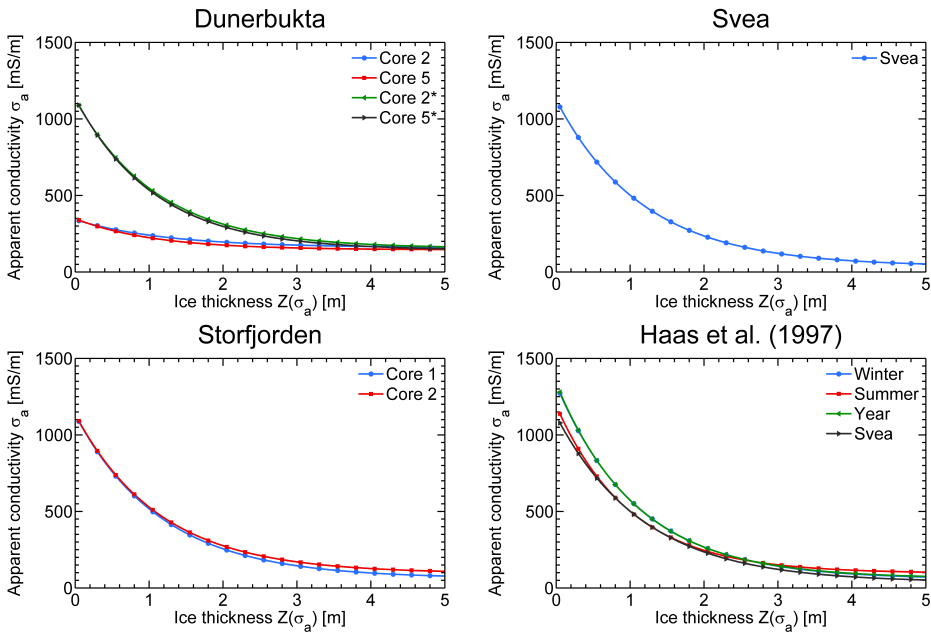
Figure 5.2: Simulated apparent conductivity and ice thickness plotted for each of the three field sites. In addition, Haas et al. (1997) formulas have been plotted. In Dunérbukta, both the $\sigma_{sw} = 500mS/m$ and $\sigma_{sw} = 2700mS/m$ where the last is marked with a star.

5.1.2 Influence of conductivity profile scaling

In Figure 5.3 Algorithms 3 and 4 have been applied to the conductivity profile of Core 5 in Dunérbukta, with both $\sigma_{sw} = 500mS/m$ and $\sigma_{sw} = 2700mS/m$. The method have been applied to all of the cores and shows that the algorithms have a large impact on the results. Both algorithms have the same response when the ice is ≈ 0, and from there move towards

different asymptotes as the thickness increases. This is because the different algorithms will give the same average conductivity of the ice for infinite thickness. In order to decide which one of these two algorithms that is the best, more experiments and calculations needs to be done. In addition, most probably better algorithms can be developed, taking into account the physical processes as brine movement and temperature profiles. Another aspect that can be added to such an algorithm is the snow thickness, and the effect on both instrument height and temperature profile.
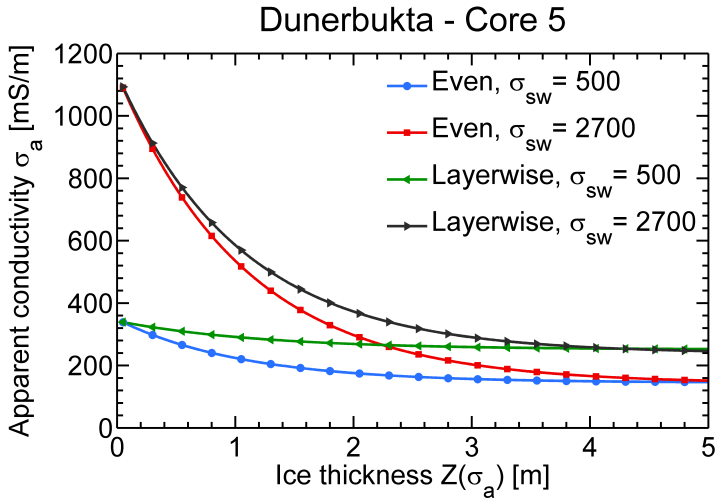
Figure 5.3: Comparison of the two level ice scaling algorithms proposed. Core 5 from Dunérbukta is used as an example, with both $\sigma_{sw} = 500mS/m$ and $\sigma_{sw} = 2700mS/m$ shown.

5.2 Applying calculated $Z(\sigma_a)$ on level ice

To investigate the significance of the calculated coefficients, the ice thickness of level ice has been calculated for all three areas.

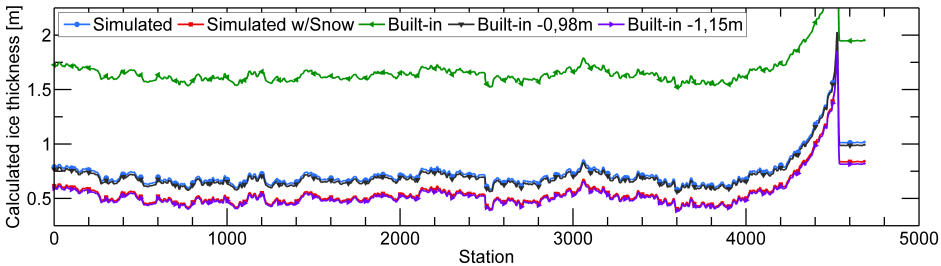### 5.2.1 Sveasundet

The $Z(\sigma_a)$ coefficients has been calculated for both the instrument height (98 cm), and the instrument height + average snow thickness (115,2 cm) and sea water conductivity of 2700 mS/m. This gives the following equations

$$Z(\sigma_a)_{98cm} = 7,802 - \ln(\sigma_a - 24,85)/0,806 \tag{5.1a}$$
$$Z(\sigma_a)_{115,2cm} = 7,762 - \ln(\sigma_a - 22,60)/0,792 \tag{5.1b}$$

where the snow is treated as having the same conductivity as air. These equations have been applied to the measured apparent conductivities, plotted in Figure 5.4. The built in ice thickness calculation is also plotted, for both the direct results, the results minus the height of the instrument, and minus the average snow thickness. The difference between the built in-thickness calculation and the calculated formula is 1,6 and 2,3 cm with and without snow respectively. The average ice thickness from drilling is 79 cm, which both calculations misses with more than 20 cm when the snow thickness is considered. This is most probably due to the sea water conductivity used in the simulation is larger than the actual conductivity.

Figure 5.4: Ice thickness calculated from the transect in Sveasundet. The blue and red line is the results from Equation 5.1, and the rest is from the built-in software.

If one regards the drastic increase in ice thickness calculated near the end of the transect, this is believed to be an effect of the ice being grounded or nearly grounded in the area, as indicated by the drilling. The influence of the ground under the ice, makes the ice to appear thicker. The flat part is when the instrument was standing on the ground.

5.2.2 Storfjorden - Walkabout

The same method have been applied to the EM31-Walkabout in Storfjorden. As both snow and ice thickness measurements are missing, the measurements cannot be verified. It can however give a pointer to say how much this method differs from using the standard calculations. Using the simulated equations, the average thickness was 84, 86 and 65 cm from core 1, core2 and built-in calculation respectively. The difference between the two cores (1 and 2) is 2,4cm and between core 1 and built-in calculation was 18,8cm. This indicated that there is a significant difference between the two methods, which needs to be investigated.

5.2.3 Dunérbukta

In Dunérbukta, the same procedure was conducted using Core 5, with $\sigma_{sw} = 2700mS/m$ with similar results. In addition to the previous calculation, the simulated formula has been found for each snow depth, as described in Algorithm 5.5a in Section 3.4.4. The results from this method is shown in Figure 5.5. The difference between calculating the

coefficients for each point and calculating one for all is shown in Figure 5.5b, where the difference between the two methods varies from 0 to 35 cm.

The idea behind this method is to utilize the advantage of simulation. Field calibration cannot be done for each points height in the same way, and therefore this method makes good use of the snow depth data usually collected. It allows the surveyor to make an interpolation model of the snow layer, and compensating for it. This method is by no means done, and need more testing and calibration. However, the method has a potential to give more accurate information of ice thickness. It should also be noted that the freeboard was negative for the most of the grid, and the slush layer on top will affect the readings greatly.
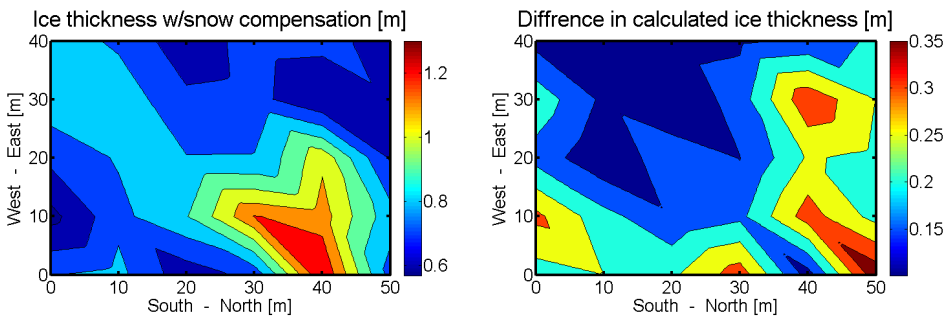

Figure 5.5: Measured grid in Dunérbukta where, **a)** Ice thickness is calculated using Algorithm 5 and **b)** Difference between snow compensated and not compensated calculation of ice thickness is shown.

5.3 Applying calculated $Z(\sigma_a)$ on ice ridge

The calculated equations have been applied to the measurements on the ridge. The ridge is quite small, and it is questionable whether or not it can be called a ridge at all. The macro porosity is also nill. The combination of these factors makes the ridge unsuited to validate the methods that will apply to ridges thicker than 3-4 meters. It is however well suited to test the simulation approach to measure level ice. This method has been applied for all of the measured data, and Section C is plotted in Figure 5.6, where the ice thickness is calculated using the data from Core 1 and 2 (blue and red) with the EM31 in parallel position. In order to compare with normal methods, Haas et al. (1997) winter formula is also applied (green). The black and grey are the ice and the ice and snow thickness combined from drilling.

As can be seen in Figure 5.6, both the calculation from Core 1 and 2 fits the drilled data quite well, and better then the calculations done with Haas et al. (1997) winter formula. On the level ice (station 4–8) the Core 1 and 2 is within centimetres of the drilled thickness, and 20 cm closer then the winter equation. Remembering that Core 2 was taken in this area, this makes a strong case for this method on level ice. Closer to the ridge (station 2-3) the "bleeding" from the footprint is clear as the Keel and Sail is within the footprint. On
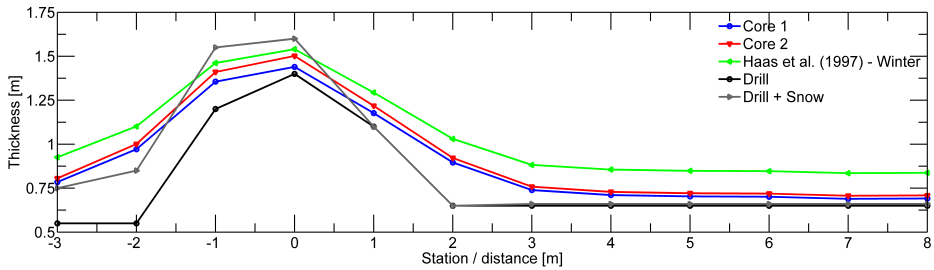
Figure 5.6: Calculated ice thickness of Section C on the ice ridge in Storfjorden. The thickness is calculated with data from Core 1 (blue), Core 2 (red), and Haas et al. (1997) (green) in addition to sea water conductivity from the CTD. The black and grey are the ice and the ice and snow thickness combined from drilling respectively
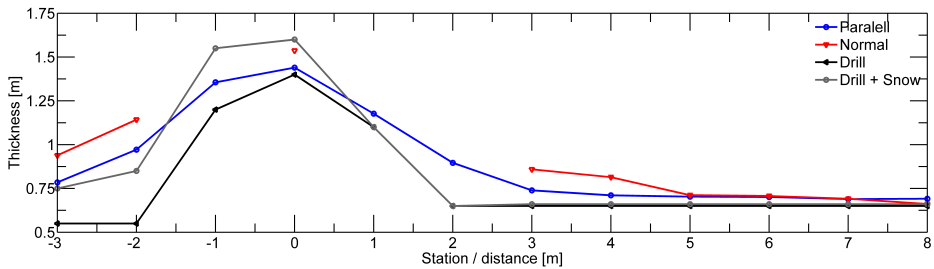
**Figure 5.7:** Calculated ice thickness of Section C on the ridge in Storfjorden in parallel (blue) and normal (red) orientation. The thickness is calculated using the simulated formula from Core 1. The black and grey are the ice and the ice and snow thickness combined from drilling respectively. Note that some of the data in the normal position is missing, as it was impossible to measure in that position.

the other side of the ridge the calculated thickness is much worse, due to the thick snow layer. If one includes the snow layer in the calculations, the calculated thickness fits much better. Regarding the EM31 in the normal position, the results from this is much more stretched. This is because the footprint than is oriented normal to the ridge, and the spatial dimension in that direction is less then in the parallel. This can be seen in Figure 5.7, where the parallel and normal orientation is plotted against each other, using the simulated equation from Core 1.

5.4 Level ice model of ice ridge

The model described in Section 3.4.5 has been calculated and shown in Figure 5.8. The ridge is simulated with an keel depth of 6,5 meters, giving a total thickness at the centre of 7,56 meters. The red lines are macro porosities 0%, 30% and 60%, and the blue lines are 10%, 20%, 40%, and 50%. The calculated response from the 12 layer cumulative response function shown in Figure 5.8a shows a conductivity much higher than expected. This is believed to be an effect of the small numbers approximation being violated. In Figure 5.8b the similar results from level ice modelling with MarcoAir are shown. Here the results are more as expected, and the point where the sail starts is clearly visible. At the centre, all the different porosities are approaching the same conductivity as expected, when the ice thickness is larger than 4 meters. Notice how the macro porosity affects the apparent conductivity in the area, where the sail is not, as this area is where it is more easy to differentiate the macro porosities.

The thickness calculated from the apparent conductivity in 5.8b is shown in Figure 5.8c. The calculation is conducted with Equation 2.22c, the year average equation by Haas et al. (1997). As expected, the greater the macro porosity, the thinner the ice appears to the EM31. The effect is up to more than one meter just before the sail starts. This effect can be used if one know the thickness and conductivity of the ice in order to approximate the macro porosity. Closer to the centre of the ridge, the thickness increases dramatically due to the asymptote of the equation. The asymptote is $\sigma_a = 62,5mSm$, where the logarithm is undefined. If the apparent conductivity becomes smaller than that, the equation breaks down.
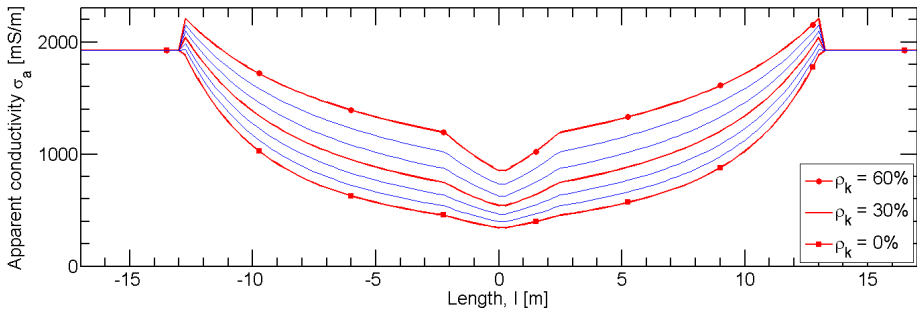
(a) Apparent conductivity from cumulative response.
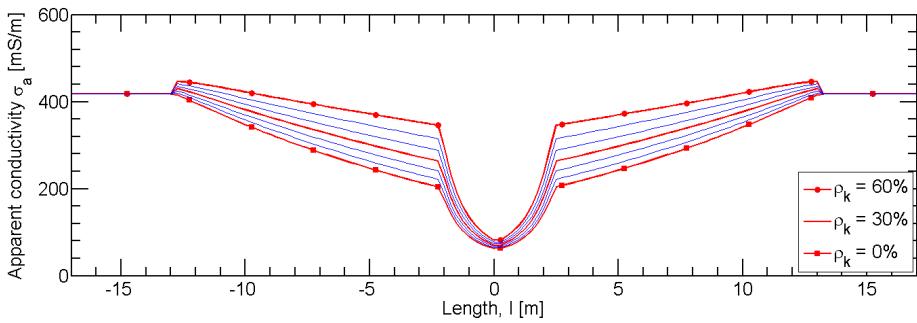
(b) Apparent conductivity from level ice modelling in MarcoAir.
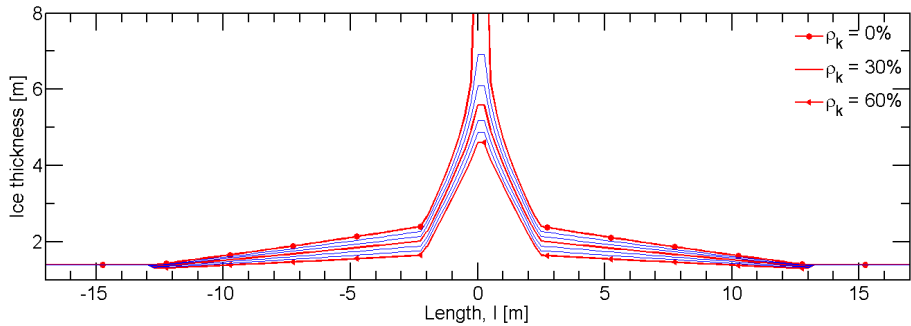
(c) Calculated thickness from apparent conductivity from MarcoAir modelling.

Figure 5.8: Simulation of the response of EM31 taken at an instrument height of 0.14 m over an average ice ridge with a keel depth of 6.5 meters. The graphs **(a)** and **(b)** shows the response using the Cumulative method and simulation of level ice using MarcoAir at porosities 0%, 10%, 20%, 30%, 40%, 50% and 60% respectively. Graph **(c)** shows the calculated thickness calculated from **(b)** using Equation 2.22c.

Chapter 6

Discussion

6.1 Simulation based calculations of $Z(\sigma_a)$ parameters

The methods developed in order to simulate the relationship between the apparent conductivity and the sea ice thickness has shown to be as accurate or more so than the methods applied by Haas et al. (1997). This indicates that this method potentially can improve the measurements of level ice in the future, and increase fieldwork efficiency. It does need more validation before it can be set into wide spread use.

As seen in the analysis, the sea ice conductivity affects the thickness measured, and more the thicker the ice is. This is because a larger part of the half-space is filled with sea ice. On the other hand, for really thin ice, the sea ice conductivity has only marginal influence. It will nonetheless be important to include the conductivity in the calculations to identify thicker ice.

Compensating for the snow layer can theoretically improve the accuracy of measurements of snow covered ice. These methods can potentially also include automatic identification of a slush layer by including freeboard in the data input. If the freeboard is negative, there can be assumed to be a slush layer on top of the ice. As this layer has a higher conductivity than snow, including it will be important.

6.2 Potential methods of estimating internal structure of an ice ridge.

There are many potential ways of estimating the internal structure of an ice ridge, depending on which other measurements that is available. There are multiple possible combinations, and standards of using the EM31. Apart from carrying the EM31 and making manual

measurements, the EM31 is often mounted on ships with a laser range finder (Haas, 1998; Reid et al., 2002, 2003; Uto et al., 2006), or the EM31 is hung from an helicopter. For the airborne application, other systems is usually applied, but following the same principles as the EM31 (Reid et al., 2006a; Haas et al., 2009). Bjerkås (2006) mounted the EM31 on a lighthouse, with a laser range finder and an echo sounder. Without knowing the instrument height over the ice, it will be significantly harder to estimate the porosity. The depth of the keel is also an important parameter in these calculations and methods and needs to be either directly measured, or estimated.

The two internal properties of a ice ridge most likely to be successfully estimated using the EM31, is the thickness of the consolidated layer, and the macro porosity. The thickness of the consolidated layer has not been the main focus of this thesis. However as the thickness of the consolidated layer is important to the calculation of the macro porosity and proposal for a method of calculating it is included. The thickness of the consolidated layer is used in the ice ridge model required to calculate the macro porosity.

6.2.1 The consolidated layer

To calculate and find the thickness of the consolidated layer, using an combination of pattern recognition, signal analysis and known factors are proposed. The thickness of the consolidated layer can be estimated by considering the average level ice thickness in the area, the minimum thickness measured by both the EM31 and the other methods in combination with the statistics available. This method need much more development before it can be applied.

6.2.2 The macro porosity

In order to estimate the macro porosity, the main idea is to compare the apparent conductivity profile with the profile expected from an solid ice block. The process can be broken down into two steps: 1) Make a geometric and conductivity model of the ice ridge and 2) Compare the results and calculate the macro porosity. In order to make a model of the ice ridge, there is different options depending on what measurements that is available. The best measurements will be a data set containing the EM31, snow, drilled thickness and sonar from below. Potentially also sail profile from a laser measurement. The proposed different ways of constructing the model is:

EM + laser is the method that usually is applied to ships. Using these two data sets in combination with the standard shape factors, one can make a simple model of the ice ridge. The keel depth can be estimated from the width of the keel, width of the sail, and sail height. Both these dimensions will be possible to distinguish with a combination of the two measurements using signal analysis methods. This can give a simplistic model of the ridge.

EM + drilling + snow is the method that corresponds to in situ investigation. From these measurements it is quite easy to make an model of the ridge, as the drilling will give the thickness profile directly, and the snow will give the offset of the EM31.

EM + sonar + laser corresponds to the work done by Bjerkås (2006). Much the same as above, as the total thickness of the snow and ice can be calculated by the sonar and laser measurements. Note that the snow thickness here is not measured and will affect the accuracy. This can be compensated by adding a modelled layer of snow on top, based on observation and wind direction.

All with all possible methods available, one can construct a full 2/3D model of the ridge, including macro porosity (from drilling), and validate the calculations and simulations in the second step of the process.

Other combinations than these four exist, but is not discussed here.

The second step is to compare the results, and calculate the macro porosity by using the model made in the first step. In the simplest form, these calculations will be a volumetric approximations dependent on the difference between the model ice thickness and the calculated thickness from the apparent conductivity, and assuming a uniform macro porosity through the unconsolidated layer. This form of calculation can be improved by taking into account the internal structure and probabilities of the composition (ex. from Kharitonov (2008), and Strub-Klein and Sudom (2012)). Building a calculation from these factors is believed to give a good approximation of the macro porosity.

In order to enhance this method, a more demanding calculation involving simulation and inversion must be made. Reid et al. (2003) and Reid et al. (2006a) demonstrated that a simple quasi-2D simulation of an ice ridge can be made using MarcoAir. Expanding this with a more advanced model, and using LokiAir from the same P223 project, can produce a quasi-2D simulation and inversion of the ridge. The reason that LokiAir should be chosen instead of MarcoAir is that LokiAir has full 3D inversion capabilities. This method of making an estimated model, then simulating and inverting is well known in the geology and geophysics depending as it is one of the more common ways of finding mineral deposits, even though it is on a different scale. The advantage over the geophysical investigation of minerals is that the shape and sizes of an ice ridge is much more controlled, and therefore a much better model can be made from the initial data.

A small attempt of making such a model and inversion was conducted during the thesis, but due to time constraints it was not completed. The attempt was to recreate the model used by Reid et al. (2003) and add pockets of sea water into the keel to investigate the response of the EM31. Completing this model will probably be the first step in developing this method further.

Regarding the ice conductivity into these models is important, since the thicker the ice becomes, the more influence the ice conductivity has. In addition, if the macro porosity is calculated by the difference between the modelled and the measured response, then the sea ice conductivity is of direct influence to the results. For thinner ridges like the one measured in Storfjorden the equation simulated from the conductivity profile will potentially help with the accuracy of these smaller, level-ice like ridges.

Chapter 7

Conclusions

Field investigation with the EM31 device has been conducted at three different field locations, where level ice and a ice ridge has been measured. Ice core profiles and manual ice measurements has also been collected.

Simulation of the response of the EM31 on level ice and a simple ridge model has been conducted showing good results. Level ice simulation shows a clear correlation between sea ice conductivity profile and the EM31 response. Simple simulation of an ice ridge show that the ice conductivity influences the EM31 response the thicker the ridge is.

Simulation based derivation of the relationship between apparent conductivity and sea ice thickness can potentially increase the accuracy of ice thickness measurements by including snow thickness, by calculating equations for each snow thickness.

Investigation into the potential methods of estimating internal structures of ice ridges show that there is great potential in using simulation and modelling in combination with inversion in order to assess these properties. There is however need for more research and development of these methods.

Two different algorithms for stretching the conductivity profile of sea ice is presented. It is shown that the algorithm have an influences on the calculation of sea ice thickness to a certain extent.

Regarding the four questions asked in the introduction, each of them are answered below:

Question 1: The conductivity profile on the level ice has a significant effect of the response from the EM31, and it affects the ridges in a similar way. The level ice conductivity profile and bulk conductivity is important to the interpretation and modelling of ice ridges.

Question 2: It is possible to make an 3D inversion model of ice ridges and use it to estimate the internal structure of ice ridges. It does face challenges as the scale and properties of ice ridges violates most of the common assumptions.

Question 3: Good conductivity models of ice ridges can improve the estimation di-

rectly by improving both the simulation and calculation.

Question 4: It will probably be possible to make an automatic system to analyse ice ridges, but it demands a lot of research and development. If such a system is made, it can have large effects on the activity in the Arctic.

Chapter 8

Further investigation

There is a big potential for future research in the field of studying the internal structures of ice ridges by electromagnetic methods. Up to now, this has not been fully investigated Four main areas of future investigation is proposed:

Simulated level ice equation The method used to simulate and fit an equation for the level ice thickness from the conductivity profile needs validation and improvement. At the moment there is not enough validation to conclude whether or not the method is better than the standard, even though the results point in that direction. It will potentially reduce the time needed on scientific cruises, as the calibration grid required takes much time to complete.

Conductivity profile of ice ridges If the conductivity profile of an ice ridge is better understood and quantified, it will greatly improve the accuracy of the electromagnetic measurements of ice ridges.

Calculation of macro porosity w/o simulation This method has the potential to make an relative simple equation that gives the macro porosity of an ice ridge. It does however need more development and much more validation to be reliable.

Modelling and inversion of an ice ridge This is the method that both is the most demanding, need the most work and has the greatest potential. If this succeed, one can make an integrated system placed on a ship that measures the ice thickness, the size and dimension of the ridges, and the structural properties of the ridge. A system like this will have great value for shipping, and oil and gas in Arctic waters. This will also require an ice ridge detection algorithm.

All of these four topics have will improve the understanding of ice ridges and measurement of level ice. There is also potential to improve the efficiency of fieldwork in the Arctic, and map large amounts of ice ridges.

Appendices

Appendix A

Ice Ridge structure from echo sounder

In addition to the electromagnetic investigation, an attempt at investigate the structure of an ice ridge keel with an echo sounder lowered into the water has been made.

A.1 Background

During the planning phase of the thesis a method for measuring the bottom layer of the keel was of interest, and the solution, to lower a echo sounder into the sea under the ice was proposed. The plan was to use the echo sounder in combination with the CTD in order to estimate the depth of the keel. Kongsberg Maritime supplied the echo sounder EK15 and a CTD from Sea-Bird was appropriated.

A.2 Equipment and instrumentation

The experimental set-up used was an EK15 echo sounder with a $26°$ wide beam in combination with a CTD. The EK15 is a scientific echo sounder mainly used for fishery research, made by Kongsberg Maritime AS / Simrad. The EK15 echo sounder has an operational frequency of 200 kHz and is used in combination with a computer running appropriate software (Simrad, 2014). The CTD used was a Sea-Bird FastCAT 49 (SBE49) made for profiling (Sea-Bird, 2015). The SBE49 has an scanning frequency of 16 Hz, significantly more than most other systems in the same category. The SBE49 has a pump that feeds the water through the conductivity and temperature sensors. The maximum operation depth of the instrument is 200 meters, limited by the depth sensor and the plastic hull.

Figure A.1: Use of the EK15 and SBE49 at the iceberg in Storfjorden. The instruments is lowered into the hole. The box contains the power supply and the computer logging the measurements.

These two instruments where fastened together and lowered into the water, as shown in Figure A.1. In Storfjorden, a long stick (approx 7m) long also was used in an attempt to direct the echo sounder. The two instruments where connected to the field computer on the top of the ice, and the data capture was synchronised. In Storfjorden, also an underwater camera was mounted in order to investigate the strange results.

The data capture and processing demanded that a new interface of the SBE49 was written in order to make the data capture synchronised, as the time handling in the standard software was not sufficient. This new interface was written in Phyton 2.7 (Rossum and Drake, 2001) with the help of the PySerial package (Liechti, 2013). This development demanded quite some time to accomplish.

A.3 Results and discussion

The results from this attempt was rather unfulfilling. The echo sounder and the CTD was caught by the current and angled as shown in Figure A.2 in such a way that no reliable data could be gathered. The instrumental set-up was missing a fixed point in the horizontal plane to be able to produce the desired results.

In order to succeed in measuring the ice ridge keel with a echo sounder from below with a non-moored system, it is believed that the following improvements will yield results:

Fixed beam with scanner: Fastening the echo sounder on a fixed beam that is lowered down into the hole in the ice is the simplest way of solving the problems. This however is not a perfect solution as the it does not solve the problem of relative position. If one adds a scanner (ex. a robotic arm), this problem is probably solved.

Multi-beam sonar: Probably the best solution is to to replace the echo sounder with an multi-beam sonar. This will give a 3D image from each position and a full 3D

Figure A.2: Picture from the video captured by the underwater camera during operation of the EK15. The picture shows the transducer angled by the current, and the guiding stick being bent.

model can be compiled.

ROV/AUV: Adding the echo sounder to a ROV or AUV has been done many times, and is a tried method.

Structure-from-motion: A more unconventional idea is to use Structure-from-motion (Westobya et al., 2012) to make a 3D model of the keel. With a couple of references or the location of each photo, a 3D model can be compiled rather accurately. This method require an underwater camera and good underwater visibility.

The method appears to have potential, but this attempt did not yield any results.

Bibliography

Archie, G., 1942. The electrical resistivity log as an aid in determining some reservoir characteristics. Trans. Am. Inst. Min. Metall. Pet. Eng. 146, 54–62.

Arya, S. P. S., 1973. Contribution of form drag on pressure ridges to the air stress on arctic ice. Journal of Geophysical Research 78 (30), 7092–2202.

Berkman, P. A., Young, O. R., April 2009. Governance and environmental change in the arctic ocean. Science 324 (5925), 339–340.

Bjerkås, M., 2006. Ice actions on offshore structures. Ph.D. thesis, Norwegian University of Science and Technology.

Eicken, H., October 1992. Salinity profiles of antarctic sea ice: Field data and model results. Journal of Geophysical Research 97 (C10), 15,545–15,557.

Eicken, H., 2009. Field Techniques for Sea-Ice Research. University of Alaska Press.

Frankenstein, G., Garner, R., 1967. Equations for determining the brine volume of sea ice from -0.5$^\circ C$ to -22.9$^\circ C$. Journal of Glaciology 6 (48), 943–944.

Garbrecht, T., Lüpkes, C., Augstein, E., Wamser, C., October 1999. Influence of a sea ice ridge on low-level airflow. Journal of Geophysical Research: Atmospheres 104 (Issue D40), 24499Ű24507.

Golden, K. M., Eicken, H., Heaton, A. L., Miner, J., Pringle, D. J., Zhu, J., 2007. Thermal evolution of permeability and microstructure in sea ice. Geophysical Research Letters 34, L16501.

Haas, C., 1998. Evaluation of ship-based electromagnetic-inductive thickness measurements of summer sea-ice in the bellingshausen and amundsen seas. Cold Regions Science and Technology 27.

Haas, C., Gerland, S., Eicken, H., Miller, H., 1997. Comparison of sea-ice thickness measurements under summer and winter conditions in the arctic using a small electromagnetic induction device. Geophysics 62 (3), 749–757.

Haas, C., Lobachb, J., Hendricksa, S., Rabensteina, L., Pfafflinga, A., 2009. Helicopter-borne measurements of sea ice thickness, using a small and lightweight, digital em system. Journal of Applied Geophysics 67 (3), 234–241.

Hall, C. M., 2001. Trends in ocean and coastal tourism: the end of the last frontier? Ocean & Coastal Management 44 (9-10), 601–68.

Hopkins, M. A., Tuhkuri, J., 1999. Compression of floating ice fields. Journal of Geophysical Research 104 (C7), 15,815–15,825.

Høyland, K. V., 2002a. Consolidation of first-year sea ice ridges. Journal of Geophysical Research 107 (C6).

Høyland, K. V., May 2002b. Simulations of the consolidation process in first-year sea ice ridges. Cold Regions Science and Technology 34 (3), 143–158.

Høyland, K. V., 2009. Ice thickness, growth and salinity in van mijenfjorden, svalbard, norway. Polar Research.

Ingham, M., Gouws, G., Buchanan, S., Brown, R., Haskell, T., 2012. In-situ measurements of the low frequency dielectric permittivity of first-year antarctic sea ice. Cold Regions Science and Technology.

Jaklin, G. S. (Ed.), 2003. The Place Names of Svalbard. Norwegian Polar Institute, Norwegian Polar Institute, Polar Environment Centre, N-9296 Tromsø, NORWAY.
URL http://stadnamn.npolar.no/stadnamn

Kharitonov, V. V., May 2008. Internal structure of ice ridges and stamukhas based on thermal drilling data. Cold Regions Science and Technology 52 (3), 302–325.

Kovacs, A., Diemand, D., Bayer, jr, J. J., June 1996. Electromagnetic induction sounding of sea ice thickness. Tech. Rep. 96-6, Cold Regions Research and Engineering Laboratory (CRREL).

Leppäranta, M., Lensub, M., Kosloffb, P., Veitchc, B., May 1995. The life story of a first-year sea ice ridge. Cold Regions Science and Technology 23 (3), 279–290.

Liechti, C., 2013. PySerial, 2nd Edition. SourceForges.
URL http://pyserial.sourceforge.net/

Løset, S., Shkhinek, K. N., Gudmestad, O. T., Høyland, K. V., 2006. Actions from Ice on Arctic Offshore and Coastal Structures. LAN St. Petersburg, ISBN S-8114-0703-3, 266 p.

MATLAB, 2013. version 8.2.0.701 (R2013b). The MathWorks Inc., Massachusetts, USA.

McNeill, J. D., October 1980. Electromagnetic terrain conductivity measurement at low induction numbers. Technical Note 6, Geonics Limited.
URL http://www.geonics.com/html/technicalnotes.html

Morey, R., Kovacs, A., , Cox, G., 1984. Electromagnetic properties of sea ice. Cold Regions Science and Technology 9, 53–75.

Nabighian, M. N. (Ed.), 1987. Electromagnetic Methods in Applied Geophysics: Voume 1, Theory. Society of Exploration Geophysicists.

Norwegian Polar Institute, 2015. Topo Svalbard. Website, Accessed on 2015/03/24.
    URL http://toposvalbard.npolar.no/

Palmer, A., Croasdale, K., October 2012. Arctic Offshore Engineering. World Scientific Publishing Co., iSBN: 9789814368773.
    URL http://ask.bibsys.no/ask/action/show?pid=141221704&
    kid=biblio

Parmeter, R., Coon, M. D., 1972. Model of pressure ridge formation in sea ice. Journal of Geophysical Research 77 (33).

Piechura, J., Walczowski, W., 2009. Warming of the west spitsbergen current and sea ice north of svalbard. Oceanologia 51 (2), 147–164.

Raiche, A., 2008. P223 prodject. Tech. rep., Commonwealth Scientific and Industrial Research Organisation (CSIRO).
    URL http://p223suite.sourceforge.net/

Raiche, A., Sugeng, F., January 2008. P223 em modelling projects. Tech. rep., Commonwealth Scientific and Industrial Research Organisation (CSIRO) and AMIRA International.
    URL http://www.amirainternational.com/WEB/site.asp?
    section=news&page=projectpages/p223f_software

Reid, J., Kimber, B., Worby, A., 2002. A calibration procedure for ship-borne em31 sea ice thickness measurements. In: Ice in the Environment: Proceedings of the 16th IAHR International Symposium on Ice.

Reid, J. E., Pfaffling, A., Vrbancich, J., 2006a. Airborne electromagnetic footprints in 1d earths. Geophysics 71 (2), G63–G72.

Reid, J. E., Pfaffling, A., Worby, A.P. Bishop, J., 2006b. In situ measurements of the direct-current conductivity of antarctic sea ice: implications for airborne electromagnetic sounding of sea-ice thicknessl. Annals of Glaciology 44.

Reid, J. E., Worby, A. P., Vrbancich, J., Munro, A. I. S., 2003. Shipborne electromagnetic measurements of antarctic sea-ice thickness. Geophysics 68 (5), 1537–1546.

Reynolds, J. M., 2011. An Introduction to Applied and Enviormental Geophysics, 2nd Edition. Vol. 1 of 1. Jhon Wiley & Sons, Ltd.

Rossum, G. v., Drake, F. (Eds.), 2001. Phyton 2.7. PhytonLabs, Virginia, USA.
    URL http://www.python.org/

Sea-Bird, February 2015. SBE 49 FastCAT CTD Sensor - User Manual. Sea-Bird Scientific, 13431 NE 20th Street, Bellevue, Washington, 98005 USA, 017th Edition.
URL http://www.seabird.com/sbe49-fastcat-ctd

Shafrova, S., August 2007. First-year sea ice features: Investigation of ice field strength heterogeneity and modelling of ice rubble behaviour. Ph.D. thesis, Norwegian University of Science and Technology and The University Centre in Svalbard.

Shirasawa, K., Tateyama, K., Takatsuka, T., Kawamura, T., Uto, S., November 2006. Ship-borne electromagnetic induction sounding of sea ice thickness in the arctic during summer 2003. Polar Meteorology and Glaciology 20, 53–61.
URL http://hdl.handle.net/2115/38912

Simrad, May 2014. Simrad EK15 Reference manual. Kongsberg Maritime AS / Simrad, Strandpromenaden 50, 3190 Horten, Norway, Rev. C, ISBN-13: 978-82-8066-142-5.
URL http://www.simrad.com/ek15

Spies, B. R., Eggers, D. E., 1986. The use and misuse of apparent resistivity in electromagnetic methods. Geophysics 51 (7), 1462–1471.

Stogryn, Desargant, 1985. The dielectric properties of brine in sea ice at microwave frequencies. IEEE Trans. on Antennas and Propagation AP-33, 523–532.

Stroeve, J. C., Markus, T., Boisvert, L., Miller, J., Barrett, A., 2014. Changes in arctic melt season and implications for sea ice loss. Geophysical Research Letters 4 (4), 1216–1225.

Strub-Klein, L., Sudom, D., 2012. A comprehensive analysis of the morphology of first-year sea ice ridges. Cold Regions Science and Technology 82, 94–109.

Tateyama, K., Shirasawa, K., Uto, S., Kawamura, T., Toyota, T., Enomoto, H., 2006. Standardization of electromagnetic-induction measurements of sea-ice thickness in polar and subpolar seas. Annals of Glaciology 44 (1), 240–246.
URL http://hdl.handle.net/2115/38910

Tateyama, K., Uto, S., Shirakawa, K., Enomoto, H., 2004. Electromagnetic-inductive measurements for the undeformed and deformed sea-ice and snow in the east antarctic. In: Proceedings of The Fourteenth (2004) International Offshore and Polar Engineering Conference. pp. 806–812.
URL http://hdl.handle.net/10213/1322

Telford, W. M., Geldart, L. P., Sheriff, R. E., 1990. Applied Geophysics, 2nd Edition. Vol. 1. Cambridge University Press.

Thomas, D. N., Dieckmann, G. S. (Eds.), 2010. Sea Ice, 2nd Edition. John Wiley & Sons.
URL http://onlinelibrary.wiley.com/book/10.1002/9781444317145

Thyssen, F., Kohnen, H., Cowan, M., Timco, G., 1974. Dc resistivity measurernents on the sea ice near pond inlet, n.w.t. (baffin island). Polarforschung 44, 117–126.

Timco, G., Burden, R., 1997. An analysis of the shapes of sea ice ridges. Cold Regions Science and Technology 25, 65–77.

Uto, S., Toyota, T., Shimoda, H., Tateyama, K., Shirasawa, K., 2006. Ship-borne electromagnetic induction sounding of sea-ice thickness in the southern sea of okhotsk. Annals of Glaciology 44 (1), 253–260.
URL http://hdl.handle.net/2115/38911

Wells, N. C., 12 2011. Atmosphere and Ocean: A Physical Introduction, 3rd Edition. John Wiley & Sons.
URL http://site.ebrary.com/lib/ntnu/detail.action?docID=10522343

Westobya, M., Brasingtonb, J., Glassera, N., Hambreya, M., Reynoldsc, J., December 2012. Śstructure.from-motionŠ photogrammetry: A low-cost, effective tool for geoscience applications. Geomorphology 179, 300–314.

WMO, 2009. Sea ice nomenclature (WMO –No.259 Suppl.No.5). Tech. rep., World Meteorological Organization.
URL http://www.jcomm.info/index.php?option=com_oe&task=viewDocumentRecord&docID=4438

Worby, A., Griffin, P., Lytle, V., Massom, R., 1999. On the use of electromagnetic induction sounding to determine winter and spring sea ice thickness in the antarctic. Cold Regions Science and Technology 29, 49–58.

Xiong, Z., 1992. Electromagnetic modeling of 3-d structures by the method of system iteration using integral equations. Geophysics 57 (12), 1556–1561.

Xiong, Z., Tripp, A. C., 1995. A block iterative algorithm for 3-d electromagnetic modeling using integral equations with symmetrized substructures. Geophysics 60 (1).